

NUWC-NPT Technical Report 11,347
15 May 2002

Model-Based Array Processing

Albert H. Nuttall
Surface Undersea Warfare Department

Andrew J. Knight
Australian Defence Science Technology Organization

REFERENCE
LIBRARY USE ONLY



**Naval Undersea Warfare Center Division
Newport, Rhode Island**

Approved for public release; distribution is unlimited.



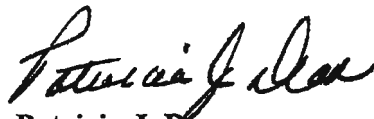
011347 001N

PREFACE

The work described in this report was sponsored by the Technical Cooperation Program (TTCP), Maritime Group, under the leadership of Bernard J. Myers (Code 01X).

The technical reviewer for this report was James B. Donald (Code 01W).

Reviewed and Approved: 15 May 2002



Patricia J. Dean

Head, Surface Undersea Warfare Department



REPORT DOCUMENTATION PAGE			Form Approved OMB No. 0704-0188
Public reporting for this collection of information is estimated to average 1 hour per response, including the time for reviewing instructions, searching existing data sources, gathering and maintaining the data needed, and completing and reviewing the collection of information. Send comments regarding this burden estimate or any other aspect of this collection of information, including suggestions for reducing this burden, to Washington Headquarters Services, Directorate for Information Operations and Reports, 1215 Jefferson Davis Highway, Suite 1204, Arlington, VA 22202-4302, and to the Office of Management and Budget, Paperwork Reduction Project (0704-0188), Washington, DC 20503.			
1. AGENCY USE ONLY (Leave blank)	2. REPORT DATE 15 May 2002	3. REPORT TYPE AND DATES COVERED	
4. TITLE AND SUBTITLE Model-Based Array Processing		5. FUNDING NUMBERS	
6. AUTHOR(S) Albert H. Nuttall Andrew J. Knight			
7. PERFORMING ORGANIZATION NAME(S) AND ADDRESS(ES) Naval Undersea Warfare Center Division 1176 Howell Street Newport, RI 02841-1708		8. PERFORMING ORGANIZATION REPORT NUMBER TR 11,347	
9. SPONSORING/MONITORING AGENCY NAME(S) AND ADDRESS(ES)		10. SPONSORING/MONITORING AGENCY REPORT NUMBER	
11. SUPPLEMENTARY NOTES			
12a. DISTRIBUTION/AVAILABILITY STATEMENT Approved for public release; distribution is unlimited.		12b. DISTRIBUTION CODE	
13. ABSTRACT (Maximum 200 words) This report discusses an array processing technique that allows optimal source amplitudes and arrival angles to be determined from the data received on arbitrary arrays. Used with either a one- or two-planewave fit to arbitrarily spaced linear arrays, the method shows superior performance to conventional beamforming when more than one source is present within the angular resolution of the array. With such situations becoming more and more likely as operating frequencies are driven to lower values, in an effort to increase detection ranges, this new approach can be used to coherently subtract strong arrivals from received data, allowing the detection of additional weak arrivals in close angular proximity. In the case where a planewave arrives at an arbitrary two-dimensional array from a moving source, a similar technique yields optimal values of the source amplitudes of the planewave, as well as the starting and ending positions of the moving source. The new processing thus performs the functions of a combined beamformer and tracker in such a way that the total error over the observation interval is minimized.			
14. SUBJECT TERMS Beamforming Methods Model-Based Processing Single Planewave Model Multiple Sources Signal Detection Double Planewave Model			15. NUMBER OF PAGES 57
17. SECURITY CLASSIFICATION OF REPORT Unclassified	18. SECURITY CLASSIFICATION OF THIS PAGE Unclassified	19. SECURITY CLASSIFICATION OF ABSTRACT Unclassified	20. LIMITATION OF ABSTRACT SAR

TABLE OF CONTENTS

Section	Page
LIST OF ILLUSTRATIONS	ii
LIST OF TABLES	iii
1 INTRODUCTION.....	1
2 ONE-PLANEWAVE FIT FOR UNEQUALLY SPACED LINE ARRAYS.....	3
2.1 Theory	3
2.1.1 Arbitrarily Spaced Line Array.....	3
2.1.2 Sparse Equispaced Line Array	7
2.2 Implementation	8
2.2.1 Coding.....	8
2.2.2 Calculation of $r(u_1)$	10
2.3 Examples.....	10
2.3.1 Noise-Free Simulations.....	10
2.3.1.1 Scenario 1: Matched Frequencies	10
2.3.1.2 Single Source Component Midway Between Fitting Bins	12
2.3.1.3 Source Component Outside the Fitting Band and Misaligned with Fitting Bins.....	12
2.3.1.4 Source Components Outside the Fitting Band and Aligned with the Fitting Bins.....	13
2.3.1.5 Source Components Outside the Fitting Band Are Misaligned, While Source Components Inside the Fitting Band Are Aligned with Fitting Bins.....	13
2.3.2 Comparison with Conventional Beamformer	15
2.3.2.1 Noise-Free Case	16
2.3.2.2 Case with Noise	18
3 TWO-PLANEWAVE FIT FOR UNEQUALLY SPACED LINE ARRAYS.....	21
3.1 Theory	21
3.2 Implementation	25
3.3 Example of Noise-Free Simulations.....	27
4 TWO-PLANEWAVE FIT TO MULTIPATH ARRIVALS FOR UNEQUALLY SPACED LINE ARRAYS	33
5 BEAMFORMING FOR A SINGLE MOVING SOURCE NEAR AN ARBITRARY PLANAR ARRAY	37
5.1 Theory	37
5.2 Implementation	40
5.2.1 Data Simulation	40
5.2.2 Example	42
5.3 Optimization Algorithm.....	43
5.4 Results.....	44

TABLE OF CONTENTS (Cont'd)

Section	Page
5.4.1 Examination of the Error Function	44
5.4.1.1 Near-Field Scenario	45
5.4.1.2 Far-Field Scenario	45
5.4.2 Fitted Trajectories with Noisy Data	46
5.4.3 Comparison with Conventional Beamformer	48
6 CONCLUSION	49
APPENDIX – ALTERNATIVE FORMULATION OF TWO-PLANEWAVE FIT	A-1
REFERENCES	R-1

LIST OF ILLUSTRATIONS

Figure	Page
1 The Result of the Maximization of r by Choice of u_1	11
2 Optimal Amplitudes for Noiseless Example	11
3 Source Frequency Midway Between Two Fitting Frequencies	12
4 Fitted Amplitudes from One-Planewave Fitting Procedure	13
5 Effect of Planewave Arrivals Outside the Fitting Band	13
6 Fitted Amplitudes with Source Frequencies Outside the Fitting Band and Misaligned with the Fitting Bins	14
7 Results of Fitting with Source Components Outside the Fitting Band and Aligned with the Fitting Bins	14
8 Results of Fitting with Source Components Outside the Fitting Band Misaligned, While Source Components Inside the Fitting Band Are Aligned with Fitting Bins	15
9 Comparison of Function $r(u_1, k)$ Equation (39) (Left) and Conventionally Beamformed Output (Right)	16
10 The Quantity $r(u_1)$ and the Sum over k of the Conventional Beamformer Output, Both Plotted as Functions of u_1	17
11 Strengths of the Fitted Frequency Components and the Amplitudes of the Conventional Beamformer Output Plotted Against Frequency Bin at $u_1 = 0.5$	17
12 The Function $r(u_1, k)$ (Equation (39)) (Left) and the Conventionally Beamformed Output (Equation (40)) (Right) for SNR of -10 dB	18
13 The Quantity $r(u_1)$ and the Sum over k of the Conventional Beamformer Output, Both Plotted as Functions of u_1	19

LIST OF ILLUSTRATIONS (Cont'd)

Figure		Page
14	Frequency Strengths Plotted Against Frequency Bin Number at $u_1 = 0.5$ for the Case with Noise.....	19
15	Conventional Beamformer Output and the One-Planewave Fit Output for Various Signal-to-Noise Ratios	20
16	Quantity $r(u_1, u_2)$ for Different Values of Source Angles u_{s1} and u_{s2}	28
17	Amplitudes of the Two-Planewaves Used for the Two-Planewave Fit	29
18	Quantity $r(u_1, u_2)$ for the Two-Planewave Fit.....	29
19	The $r(u_1, u_2)$ Surface Compared to Conventionally Beamformed Results	30
20	The $r(u_1, u_2)$ Surface Compared to Conventionally Beamformed Results for Separated Sources.....	31
21	Two-Planewave Fits and Conventional Beamforming Outputs for (a) Two Widely Separated Sources and (b) A Single Source.....	32
22	Sensor and Target Motion.....	37
23	Simulated Data.....	42
24	Error for Near-Field Scenario	45
25	Error for Far-Field Scenario.....	46
26	True Trajectory and Fitted Trajectories for Scenarios with Various SNRs	47
27	Fitted Coordinate Errors Plotted Against SNR.....	47
28	Conventionally Beamformed Results for a Stationary Source (Top) and a Moving Source (Bottom).....	48

LIST OF TABLES

Table	Page
1 Optimal Amplitude Errors for Noiseless Example	12

MODEL-BASED ARRAY PROCESSING

1. INTRODUCTION

Sonar systems are being driven to use ever lower frequencies to compensate for the quieting of acoustic emissions from targets of interest. Because these low-frequency sounds are more difficult to suppress at the source and thus can propagate further through the underwater medium, reasonable detection ranges can be maintained.

For a given sonar receiver and processing chain, the beamwidth of the system increases as the frequency decreases. As the beams become broader, there is a greater chance that more than one acoustic source will be present in the same beam. This report introduces beamforming methods that are aimed at detecting more than one source within a single beam. The techniques are based on planewave models and use fitting procedures to find optimal sets of planewaves, in a minimal squared-error sense, to match measured time series data.

Each of the following sections first presents the theoretical development and then discusses the results with simulated data, comparing these results with conventional beamforming techniques.

In section 2, a single or one-planewave model is fitted to data observed by a line array of sensors that can be arbitrarily spaced; also discussed is the special case of a sparse equispaced array.

In section 3, a two-planewave model is fitted to linear array data (arbitrarily spaced). Section 4 applies a similar technique to the situation where the two planewaves are related by a single change in amplitude and a time delay. This case represents the arrival of two planewaves from a single source via two different propagation paths (multipath).

Finally, in section 5, a model is fitted of a planewave arriving at an arbitrarily spaced two-dimensional array from a moving source. In this case, the fitting procedure yields two-dimensional start and end positions of the source, and indicates the strengths of its frequency components.

Model-based processing can be used as a preprocessor prior to such additional beamforming as conventional, adaptive, Fourier Integral Method (FIM), etc. If a double source is found, the stronger one can be coherently removed, using the modeled coefficients yielded by the fitting procedure, to better identify the weaker source(s). Removed sources can be added to subsequent sonar displays to prevent loss of information to operators.

2. ONE-PLANEWAVE FIT FOR UNEQUALLY SPACED LINE ARRAYS

2.1 THEORY

2.1.1 Arbitrarily Spaced Line Array

A continuous pressure field $\tilde{p}(t, x)$ is assumed at time t and location x . Time samples are taken at $t = n\Delta$ for $n = 0:N-1$, and spatial samples are taken at locations $x = x(m)$ for $m = 0:M-1$. The colon symbol $J:K$ is used to denote $\{J, J+1, \dots, K\}$ with $J < K$. The total discrete data available are $p(n, m) \equiv \tilde{p}(n\Delta, x(m))$ for $n = 0:N-1$, $m = 0:M-1$.

If a single planewave arrives from angle $u_1 = \sin \theta_1$ comprised of frequencies $\{f_1(k)\}_{k_a}^{k_b}$, the observed complex pressure field at (t, x) is modeled as

$$\tilde{p}_1(t, x) = \sum_{k=k_a}^{k_b} a_1(k) \exp[i 2\pi f_1(k)(t - \frac{x}{c}u_1)], \quad (1)$$

where the hypothesized amplitudes $\{a_1(k)\}_{k_a}^{k_b}$ are complex. For given frequencies $\{f_1(k)\}_{k_a}^{k_b}$ and arrival angle u_1 , amplitudes $\{a_1(k)\}_{k_a}^{k_b}$ should be chosen so that the total weighted fitting error e is minimized. Here, error is defined as

$$\begin{aligned} e &= \sum_{n=0}^{N-1} \sum_{m=0}^{M-1} w_t(n) w_x(m) \left| \overbrace{\tilde{p}(n\Delta, x(m))}^{\text{data}} - \overbrace{\tilde{p}_1(n\Delta, x(m))}^{\text{fit}} \right|^2 \\ &= \sum_{n,m} w_t(n) w_x(m) \left| p(n, m) - \sum_k a_1(k) \exp\{i \alpha_1(k) [n - \beta(m)u_1]\} \right|^2, \end{aligned} \quad (2)$$

where the temporal and spatial weights, $\{w_t(n)\}$ and $\{w_x(m)\}$, are real and positive, and the known dimensionless parameters are

$$\alpha_1(k) \equiv 2\pi f_1(k)\Delta, \quad \beta(m) \equiv \frac{x(m)}{c\Delta}. \quad (3)$$

To minimize e , Kay's partial derivative procedure¹ is used; thus,

$$\begin{aligned} \frac{\partial e}{\partial a_1^*(\underline{k})} &= - \sum_{n,m} w_t(n) w_x(m) \left[p(n, m) - \sum_k a_1(k) \exp\{i \alpha_1(k) [n - \beta(m)u_1]\} \right] \\ &\quad \times \exp\{-i \alpha_1(\underline{k}) [n - \beta(m)u_1]\} \quad \text{for } \underline{k} = k_a : k_b. \end{aligned} \quad (4)$$

The temporal and spatial windows are defined as

$$W_t(\alpha) = \sum_{n=0}^{N-1} w_t(n) \exp(-i \alpha n) \quad \text{for all } \alpha, \quad W_t(0) = 1, \quad (5)$$

$$W_x(\gamma) = \sum_{m=0}^{M-1} w_x(m) \exp(i \beta(m)\gamma) \quad \text{for all } \gamma, \quad W_x(0) = 1, \quad (6)$$

and the two-dimensional data spectrum as

$$P(\alpha, \gamma) = \sum_{n=0}^{N-1} \sum_{m=0}^{M-1} w_t(n) w_x(m) p(n, m) \exp[-i\alpha n + i\beta(m)\gamma] \quad \text{for all } \alpha, \gamma. \quad (7)$$

Then, from equation (4), the conditionally optimal complex amplitudes $\{\underline{a}_1(k)\}_{k_a}^{k_b}$, for hypothesized arrival angle u_1 , satisfy the simultaneous linear equations

$$\begin{aligned} & \sum_{k=k_a}^{k_b} \underline{a}_1(k) W_t(\alpha_1(\underline{k}) - \alpha_1(k)) W_x([\alpha_1(\underline{k}) - \alpha_1(k)]u_1) \\ & = P(\alpha_1(\underline{k}), \alpha_1(k)u_1), \quad \text{for } \underline{k} = k_a : k_b. \end{aligned} \quad (8)$$

Henceforth, only the case of flat temporal weighting is considered:

$$w_t(n) = \frac{1}{N} \quad \text{for } n = 0 : N-1. \quad (9)$$

Then, from equation (5),

$$W_t(\alpha) = \exp(-i\alpha \frac{N-1}{2}) \frac{\sin(N\alpha/2)}{N \sin(\alpha/2)}, \quad (10)$$

from which

$$W_t(2\pi k/N) = \begin{cases} 1 & \text{for } k = 0 \\ 0 & \text{for } k \neq 0 \end{cases}, \quad |k| < N. \quad (11)$$

Also, the fitting frequencies are taken as

$$f_1(k) = \frac{k}{N\Delta} \quad \text{for } k = k_a : k_b, \quad \alpha_1(k) = 2\pi k/N, \quad (12)$$

which leads to

$$W_t(\alpha_1(\underline{k}) - \alpha_1(k)) = W_t\left(\frac{2\pi}{N}(\underline{k} - k)\right) = \delta(\underline{k} - k). \quad (13)$$

Now, an explicit solution to equation (8) can be written for the conditionally optimal amplitudes; namely,

$$\underline{a}_1(k) = P(\alpha_1(k), \alpha_1(k)u_1) \quad \text{for } k = k_a : k_b. \quad (14)$$

The conditionally minimal error then becomes

$$\begin{aligned} \underline{\varepsilon} &= \sum_{n,m} w_t(n) w_x(m) \left[p(n, m) - \sum_k \underline{a}_1(k) \exp\{i\alpha_1(k)[n - \beta(m)u_1]\} \right] p^*(n, m) \\ &= \sum_{n,m} w_t(n) w_x(m) |p(n, m)|^2 \\ &\quad - \underbrace{\sum_k \underline{a}_1(k) \sum_{n,m} w_t(n) w_x(m) p^*(n, m) \exp\{i\alpha_1(k)[n - \beta(m)u_1]\}}_{P^*(\alpha_1(k), \alpha_1(k)u_1) \text{ from equation (7)}}. \end{aligned} \quad (15)$$

Now the conditionally optimal amplitudes (equation (14)) are substituted to obtain

$$\underline{e} = \sum_{n,m} w_t(n) w_x(m) |p(n,m)|^2 - \sum_k |\underline{a}_1(k)|^2 \quad (16)$$

$$= \sum_{n,m} w_t(n) w_x(m) |p(n,m)|^2 - \underbrace{\sum_k \left| P(\alpha_1(k), \alpha_1(k)u_1) \right|^2}_{\equiv r(u_1)} \quad (17)$$

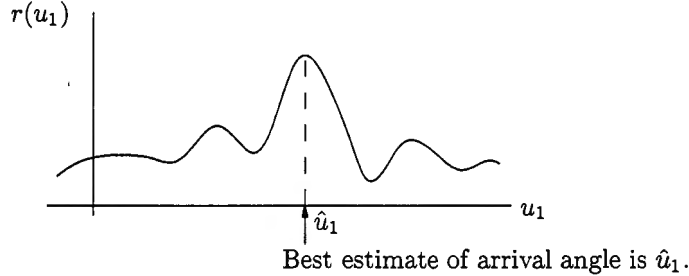
Next, the error \underline{e} is further minimized by choosing the planewave arrival angle u_1 that maximizes $r(u_1)$. Using the definition of the two-dimensional data spectrum P (equation (7)) and the flat temporal weighting (equation (9)), results in

$$\begin{aligned} r(u_1) &= \sum_k \left| \frac{1}{N} \sum_{n,m} w_x(m) p(n,m) \exp \left[-i \frac{2\pi}{N} kn + i \beta(m) \frac{2\pi}{N} ku_1 \right] \right|^2 \\ &= \sum_{k=k_a}^{k_b} \left| \sum_{m=0}^{M-1} w_x(m) q(k,m) \exp \left[i \frac{2\pi k}{N} \beta(m) u_1 \right] \right|^2, \end{aligned} \quad (18)$$

where

$$q(k,m) = \frac{1}{N} \sum_{n=0}^{N-1} p(n,m) \exp(-i2\pi kn/N) \quad \text{for } k = 0:N-1, m = 0:M-1 \quad (19)$$

is the temporal discrete Fourier transform of the m -th element data. The maximization of $r(u_1)$ by choice of u_1 is depicted in the following sketch:



The processing given by equation (18) has a very plausible form. It says to (1) first transform the time-space data $\{p(n,m)\}$ into the frequency-space domain $\{q(k,m)\}$, and then (2) for hypothesized arrival angle u_1 , scale and phase shift the m -th element component in frequency bin k by $(2\pi k/N)\beta(m)u_1$. But this phase shift exactly compensates for that of a single-frequency planewave arriving at angle u_1 :

$$\text{phase shift}(k,m) = -2\pi \frac{k}{N\Delta} \frac{x(m)}{c} u_1 = -\frac{2\pi k}{N} \beta(m) u_1. \quad (20)$$

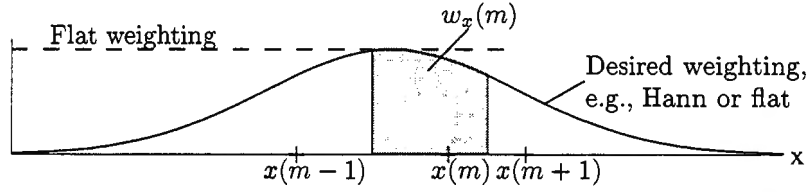
Thus, the inner complex sum over m in equation (18) is a *coherent* one for any planewave arriving at angle u_1 . Finally, the outer sum over k in equation (18) is an incoherent sum over frequencies in the band of interest. This incoherent sum is necessary because no interrelations have been assumed for individual frequency components in the planewave arrivals. After the sum over k is complete, then $r(u_1)$ is plotted for all u_1 in the angular sector of interest, and its maximum is located at \hat{u}_1 .

The complex sum on element number m in equation (18) cannot be accomplished by a fast Fourier transform (FFT) because, in general, $\beta(m) = x(m)/(c\Delta)$ is not linear in m for an unequally spaced line array (but see section 2.1.2 for a sparse equispaced line array). This complex sum must be carried out by brute force. However, one shortcut available uses the recursion

$$\exp \left[i \frac{2\pi k}{N} \beta(m) u_1 \right] = \exp \left[i \frac{2\pi(k-1)}{N} \beta(m) u_1 \right] \exp \left[i \frac{2\pi}{N} \beta(m) u_1 \right] \quad (21)$$

for each m and u_1 to generate the k -values needed for the exponentials.

Finding the best spatial weights $\{w_x(m)\}$ is not trivial; they should not simply be taken as flat but should reflect known element locations $\{x(m)\}$. For example, $w_x(m)$ might be taken to be proportional to the shaded area between adjacent element midpoints, as shown in the following sketch:



After the conditionally best coefficients $\{a_1(k)\}$ are found for a specified u_1 , the minimal conditional time-space residual is, from equations (1) and (2),

$$\begin{aligned} \underline{p}(n, m) &\equiv \tilde{p}(n\Delta, x(m)) - \tilde{p}_1(n\Delta, x(m)) \\ &= p(n, m) - \sum_k a_1(k) \exp \left[i \frac{2\pi k}{N} (n - \beta(m) u_1) \right]. \end{aligned} \quad (22)$$

The corresponding FFT of this residual is, from equation (19),

$$\begin{aligned} \underline{q}(\underline{k}, m) &= \frac{1}{N} \sum_{n=0}^{N-1} \underline{p}(n, m) \exp(-i2\pi \underline{k} n/N) \\ &= q(\underline{k}, m) - \frac{1}{N} \sum_{k=k_a}^{k_b} a_1(k) \exp \left[-i \frac{2\pi k}{N} \beta(m) u_1 \right] \underbrace{\sum_{n=0}^{N-1} \exp[-i2\pi(\underline{k} - k) n/N]}_{N\delta(\underline{k} - k)} \\ &= q(\underline{k}, m) - a_1(\underline{k}) \exp \left[-i \frac{2\pi \underline{k}}{N} \beta(m) u_1 \right], \quad \text{for } \underline{k} = k_a : k_b. \end{aligned} \quad (23)$$

The conditionally optimal amplitudes are, from equations (14), (9), (12), (7), and (19),

$$\begin{aligned} a_1(k) &= P(\alpha_1(k), \alpha_1(k) u_1) \\ &= \sum_{m=0}^{M-1} w_x(m) q(k, m) \exp \left[i \frac{2\pi k}{N} \beta(m) u_1 \right] \quad \text{for } k = k_a : k_b. \end{aligned} \quad (24)$$

These complex amplitudes should be evaluated only *after* the best arrival angle u_1 (namely \hat{u}_1) has been determined. Then, equation (23) should be evaluated, using \hat{u}_1 in place of u_1 . That is, the unconditionally optimum amplitudes are

$$\begin{aligned} \hat{a}_1(k) &= P(\alpha_1(k), \alpha_1(k) \hat{u}_1) \\ &= \sum_{m=0}^{M-1} w_x(m) q(k, m) \exp \left[i \frac{2\pi k}{N} \beta(m) \hat{u}_1 \right] \quad \text{for } k = k_a : k_b, \end{aligned} \quad (25)$$

and the minimal residual in the frequency-space domain is

$$\hat{q}(k, m) = \begin{cases} q(k, m) - \hat{a}_1(k) \exp \left[-i \frac{2\pi k}{N} \beta(m) \hat{u}_1 \right] & \text{for } k = k_a : k_b, \\ q(k, m) & \text{for } k \notin k_a : k_b. \end{cases} \quad (26)$$

Letting the spatially weighted FFT at frequency bin k be defined as

$$q_w(k, m) = q(k, m) w_x(m), \quad (27)$$

and its spatial autocorrelation for frequency bin k be defined as

$$\phi(k, j) = \sum_m q_w(k, m) q_w^*(k, m - j), \quad (28)$$

then, from equation (18), if $x(m) = d m$ (equally spaced line array),

$$\begin{aligned} r(u_1) &= \sum_{k=k_a}^{k_b} \left| \sum_{m=0}^{M-1} q_w(k, m) \exp \left[i \frac{2\pi k}{N} \frac{d m}{c\Delta} u_1 \right] \right|^2 \\ &= \sum_{k=k_a}^{k_b} \sum_{j=1-M}^{M-1} \phi(k, j) \exp \left(i \frac{2\pi k}{N} \frac{d}{c\Delta} j u_1 \right). \end{aligned} \quad (29)$$

A FIM-like²⁻⁶ generalization would be to weight the spatial sum over j to obtain the modification

$$r_s(u_1) = \sum_{k=k_a}^{k_b} \sum_{j=1-M}^{M-1} w_s(j) \phi(k, j) \exp \left(i \frac{2\pi k}{N} \frac{d}{c\Delta} j u_1 \right), \quad (30)$$

where the $\{w_s(j)\}_{1-M}^{M-1}$ are separation weights (real and even about $j = 0$).

2.1.2 Sparse Equispaced Line Array

From equation (18) with $z(m) = w_x(m)q(k, m)$ (holding k fixed), let

$$f(\nu) \equiv \sum_{m=0}^{M-1} z(m) \exp[i\nu\beta(m)], \quad \beta(m) = \frac{x(m)}{c\Delta}, \quad \nu = \frac{2\pi k}{N} u_1, \quad (31)$$

and, as an example of a sparse equispaced line array, consider

$$\begin{aligned} \{x(m)\} &= [x(0) \ x(1) \ \cdots \ x(M-1)] \\ &= [0 \ d \ \underbrace{\quad}_{1 \text{ missing}} \ 3d \ 4d \ \underbrace{\quad}_{2 \text{ missing}} \ 7d \ 8d \ 9d \ \cdots]; \end{aligned} \quad (32)$$

then

$$\{\beta(m)\} = \beta [0 \ 1 \ 3 \ 4 \ 7 \ 8 \ 9 \ \cdots], \quad \beta \equiv \frac{d}{c\Delta}, \quad (33)$$

and

$$\begin{aligned} f(\nu) &= z(0) + z(1) \exp(i\nu\beta) + z(2) \exp(i\nu\beta 3) + z(3) \exp(i\nu\beta 4) \\ &\quad + z(4) \exp(i\nu\beta 7) + z(5) \exp(i\nu\beta 8) + z(6) \exp(i\nu\beta 9) + \cdots. \end{aligned} \quad (34)$$

Letting

$$y = [z(0) \ z(1) \ 0 \ z(2) \ z(3) \ 0 \ 0 \ z(4) \ z(5) \ z(6) \ \dots], \quad (35)$$

then

$$\begin{aligned} f(\nu) &= y(0) + y(1) \exp(i\nu\beta) + y(3) \exp(i\nu3\beta) + y(4) \exp(i\nu4\beta) \\ &\quad + y(7) \exp(i\nu7\beta) + y(8) \exp(i\nu8\beta) + y(9) \exp(i\nu9\beta) + \dots \\ &= \sum_{j=0} y(j) \exp(i\nu\beta j) \\ &= \sum_{j=0} y(j) \exp \left[i2\pi \frac{k}{N} \frac{d}{c\Delta} u_1 j \right]. \end{aligned} \quad (36)$$

By taking $\frac{k}{N} \frac{d}{c\Delta} u_1 = \frac{n'}{N'}$, this process can be performed by an N' -point FFT. Sequence $\{y(j)\}$ has zeros in it, dictated by the missing element locations; as a result, the $\{z(m)\}$ are merely “spaced out” by the missing element locations.

2.2 IMPLEMENTATION

The theory outlined in the last section was implemented in a MATLAB program and tested on simulated data for a variety of scenarios.

2.2.1 Coding

The first step was to generate the data that an unequally spaced line array of sensors would produce in the presence of a planewave arriving from angle $u_1 = \sin \theta_1$. First, the source direction, frequencies, and amplitudes were defined:

```
u1_source = .5; % sin(source angle)
f1_source = 45:60; % frequencies (Hz)
a1 = [0 1 2 3 4 5 4 3 2 1 0 1 2 3 4 5]; % amplitudes
```

The fitting band and sensor parameters were also defined:

```
M = 16; % Number of sensors
wx_m = ones(1,M)/M; % spatial error weighting
ka = 45;
kb = 60;
i = sqrt(-1);
N = 1024; % Number of time points
delta = 1/1024; % sampling increment (s)
c = 1500; % sound speed (m/s)
tvect = delta*(0:N-1); % vector of sample times
rand('state',0); % Same random array each time
xarray = sort(50*rand(M,1)); % random sensor positions (m) (0,50)
```

The time-space data were then computed as a sum of planewaves at the source frequencies $f1_source$:

```
[xmatrix,tmatrix] = meshgrid(xarray,tvect);
pnm = zeros(N,M);
for k = 1:length(f1_source)
    pnm = pnm + a1(k)*exp(2*pi*f1_source(k)*...
        (tmatrix - xmatrix*u1_source/c)*i);
end
```

The next step was to find the value of u_1 that maximized $r(u_1)$ given by equation (18). First, a coarse grid search was carried out over L evenly spaced points in u_1 between -1 and 1 :

```
L = 51;
u1_l = linspace(-1,1,L);
% Calculate r(u1) using equation (17)
beta_m = xarray/(c*delta);
r_l = -calcr1(u1_l, beta_m, ka, kb, N, wx_m, pnm);
```

A subroutine `calcr1` was used to compute the values of r_l for an input vector $u1_l$, given the parameter list β_m , ka , kb , N , wx_m , and pnm (see section 2.2.2). The negative sign was used because the function `calcr1` was employed as the argument of a function-minimizing routine (see below), whereas it was required to find the function's maximum. The maximum value of r_l resulting from the coarse search and the corresponding value of $u1_l$ were found, as well as the $u1_l$ values immediately adjacent:

```
[dum,ind] = max(r_l);
if ind==1
    i1 = 1;
    i2 = 3;
elseif ind==L
    i1 = L - 2
    i2 = L;
else
    i1 = ind - 1;
    i2 = ind + 1;
end
```

(Maxima at the domain limits were handled as special cases.) An accurate estimate of the peak was obtained by using an iterative parabolic fitting routine (`FMINBND`):

```
options = optimset('TolX',1e-10);
best_u1 = fminbnd('calcr1',u1_l(i1),u1_l(i2),options,beta_m,...
    ka,kb,N,wx_m,pnm);
```

The fitting routine used the absolute tolerance set by the function `OPTIMSET`, here equal to 10^{-10} .

After the best estimate of arrival angle ($best_u1$) was found, the optimal amplitudes $\{a_1(k)\}$ were then calculated from equation (14):

```

a_1_bar = zeros(1,length(k));
[beta_m_mx,n_mx]=meshgrid(beta_m,0:(N - 1));
ik = 0;
for this_k = k
    ik = ik + 1; % index for a_1_bar;
    alpha_1_k = 2*pi*this_k/N;
    Enm = exp((-alpha_1_k*n_mx + beta_m_mx*alpha_1_k*best_u1)*i);
    Gnm = pnm.*Enm;
    Fn = wx_m*Gnm.'; % sum over m
    a_1_bar(ik) = sum(Fn)/N; % sum over n
end

```

2.2.2 Calculation of $r(u_1)$

The Fourier transform of the element data was computed explicitly for each frequency component k . A matrix product was used to perform the sum over n required in the evaluation of the transform q_{km} :

```

n = (0:(N - 1)).';
r_l = zeros(size(u1_l));
for k = ka:kb
    En = exp((-2*pi*k*n/N)*i);
    % Fourier transform at frequency k
    % (matrix product does sum over n):
    qkm = (pnm.')*En;
    E_ml = exp((2*pi*k*beta_m*u1_l/N)*i);
    % matrix product does sum over m:
    r_l = r_l + abs((wx_m.*qkm.')*E_ml).^2;
end % loop does sum over k
r_l = -r_l; % for use with MINimizer

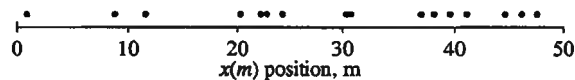
```

The negative of the final result was taken so that the routine could be used as the argument of a minimizer, as explained previously.

2.3 EXAMPLES

2.3.1 Noise-Free Simulations

2.3.1.1 Scenario 1: Matched Frequencies. The above code gave rise to $M = 16$ array elements at the following positions: $x_{array} = [0.92518, 8.8133, 11.557, 20.285, 22.235, 22.823, 24.299, 30.342, 30.772, 36.910, 38.105, 39.597, 41.070, 44.565, 46.091, 47.506]$. These positions are plotted in the following sketch:



For this example, the result of the maximization of r by choice of u_1 is shown in figure 1. In this noiseless case, the resulting estimate of \hat{u}_1 was $0.5 + 5.8 \times 10^{-11}$, yielding the optimal amplitudes $\{a_1(k)\}$, shown in figure 2.

The optimal amplitude errors, shown in table 1, are defined as $a_1(k) - \hat{a}_1(k)$. The real parts of the fitted amplitude errors are on the order of the machine precision, and the imaginary parts are of a size comparable to the tolerance on the estimation of the arrival angle (10^{-10}), except for the cases of zero amplitude, where they are of a size comparable to the machine precision. As shown in the lower plot of figure 2, the amplitudes of the imaginary parts are proportional to the real parts.

For the matched-frequency case, the set of source frequencies was equal to the set of fitting frequencies. In the following four scenarios (subsections 2.3.1.2 to 2.3.1.5), cases where the set of source frequencies is not equal to the set of fitting frequencies are considered.

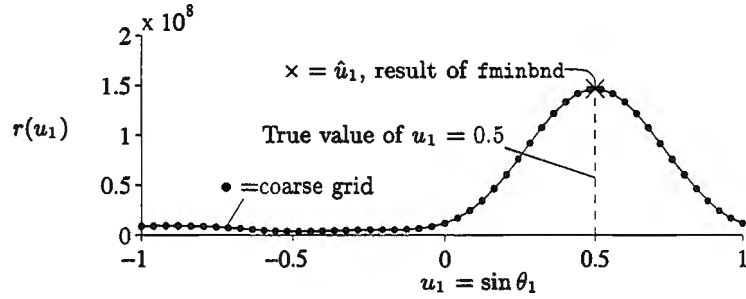


Figure 1. The Result of the Maximization of r by Choice of u_1

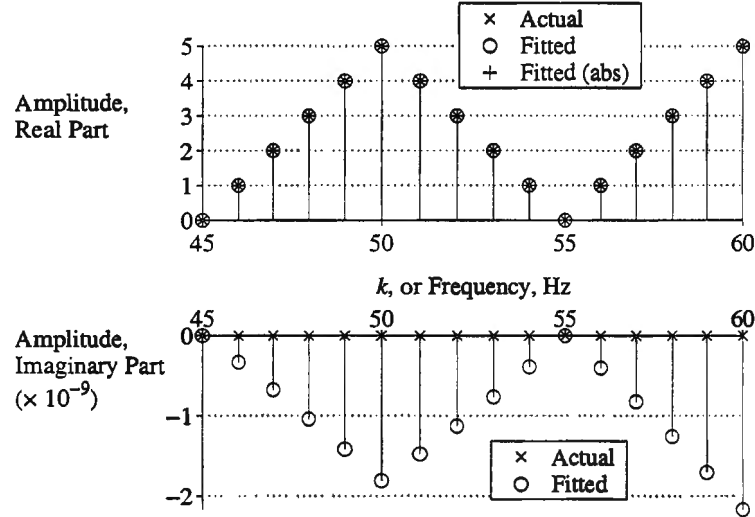


Figure 2. Optimal Amplitudes for Noiseless Example

Table 1. Optimal Amplitude Errors for Noiseless Example

k, or Frequency (Hz)	Input Amplitude, $a_1(k)$	Optimal Amplitude Error	
		Real Part	Imaginary Part
45	0	1.7×10^{-17}	5.2×10^{-15}
46	1	2.7×10^{-14}	-3.3×10^{-10}
47	2	-3.0×10^{-14}	-6.8×10^{-10}
48	3	-1.7×10^{-14}	-1.0×10^{-9}
49	4	2.5×10^{-14}	-1.4×10^{-9}
50	5	9.8×10^{-15}	-1.8×10^{-9}
51	4	0	-1.5×10^{-9}
52	3	2.1×10^{-14}	-1.1×10^{-9}
53	2	-1.9×10^{-14}	-7.7×10^{-10}
54	1	-2.4×10^{-14}	-3.9×10^{-10}
55	0	-7.6×10^{-15}	9.1×10^{-15}
56	1	-1.7×10^{-14}	-4.0×10^{-10}
57	2	7.5×10^{-15}	-8.2×10^{-10}
58	3	-1.6×10^{-14}	-1.2×10^{-9}
59	4	-2.9×10^{-14}	-1.7×10^{-9}
60	5	-3.9×10^{-14}	-2.2×10^{-9}

2.3.1.2 Single Source Component Midway Between Fitting Bins. In practice, the exact source frequencies are not known prior to conducting the single planewave fit, or the frequency bins available in an operational system may not match those of the source. To examine such a situation, the fitting procedure was run for a source frequency midway between two of the fitting frequencies, as shown in figure 3. The input angle for this case was $u_1 = 0.5$ (dashed line in the graph), and the input frequency was 52.5 Hz. The fitting frequencies were $f_k = k = 45, 46, \dots, 60$. Although the peak of the function $r(u_1)$ was found within the requested tolerance (10^{-10}), the result differed from the input angle by 3.0×10^{-4} . The fitted amplitudes in figure 4 show the leakage phenomenon typically encountered with Fourier transform processing.

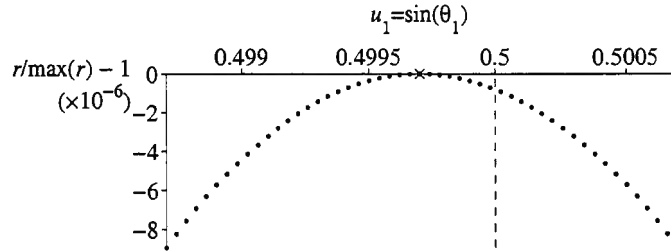


Figure 3. Source Frequency Midway Between Two Fitting Frequencies

2.3.1.3 Source Components Outside the Fitting Band and Misaligned with Fitting Bins. To investigate the effect of planewave arrivals at frequencies outside the fitting band, a set of planewaves at frequencies above and below the fitted frequencies was included. The resulting angle estimate is shown

in figure 5. The input angle for this case was again $u_1 = 0.5$ (dashed line). The fitting frequencies were $f_k = k = 45, 46, \dots, 60$. Although the peak of the function $r(u_1)$ was found within the requested tolerance (10^{-10}), the result differed from the input angle by 9.5×10^{-4} .

The fitted amplitudes are shown in figure 6. The fitted amplitudes are generally larger than the input amplitudes.

2.3.1.4 Source Components Outside the Fitting Band and Aligned with the Fitting Bins.

Figure 7 shows the effect of frequencies outside the fitting band, but this time the actual and fitted frequencies are aligned over the same equispaced Fourier bin frequencies. The angle is able to be accurately estimated by the fitting procedure, as are the amplitudes.

2.3.1.5 Source Components Outside the Fitting Band Are Misaligned, While Source Components Inside the Fitting Band Are Aligned with Fitting Bins. If the frequencies outside the fitting band are not aligned over the Fourier bin frequencies, as in figure 8, then the optimal angle and amplitudes are not able to be accurately estimated by the one-planewave fitting procedure.

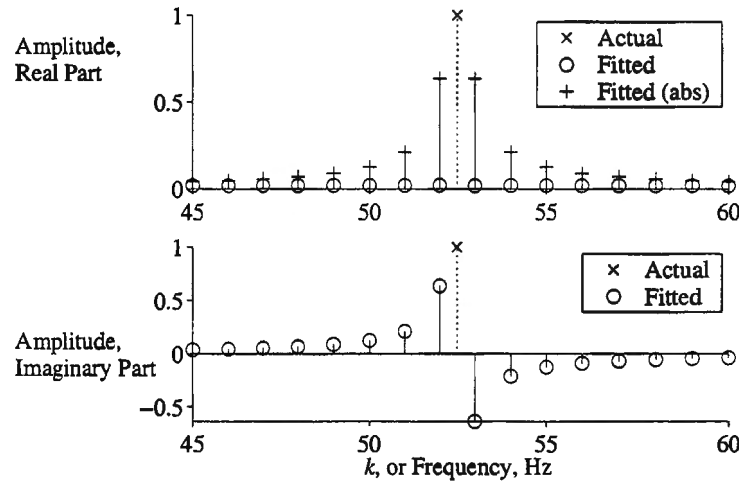


Figure 4. Fitted Amplitudes from One-Planewave Fitting Procedure

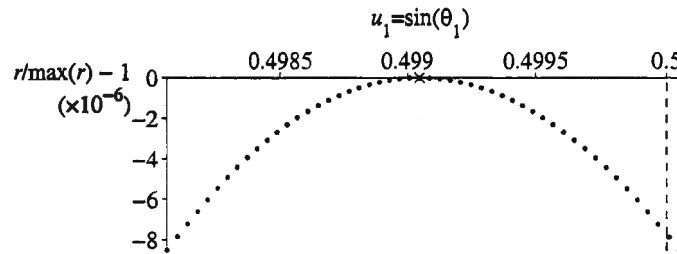


Figure 5. Effect of Planewave Arrivals Outside the Fitting Band

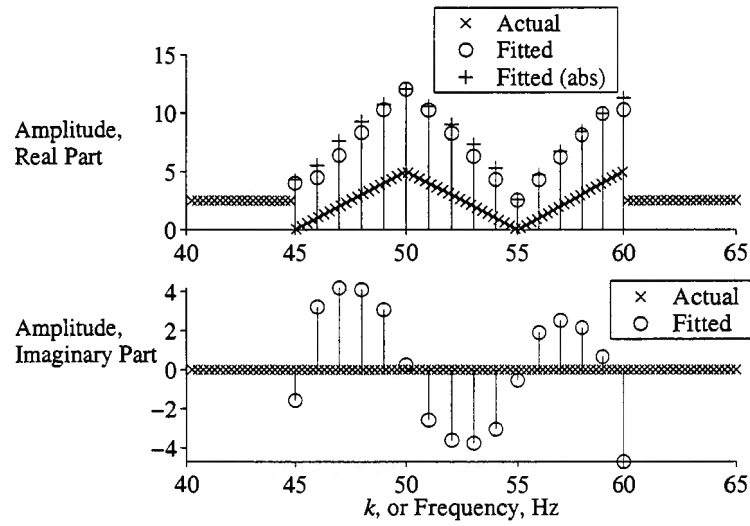


Figure 6. Fitted Amplitudes with Source Frequencies Outside the Fitting Band and Misaligned with the Fitting Bins

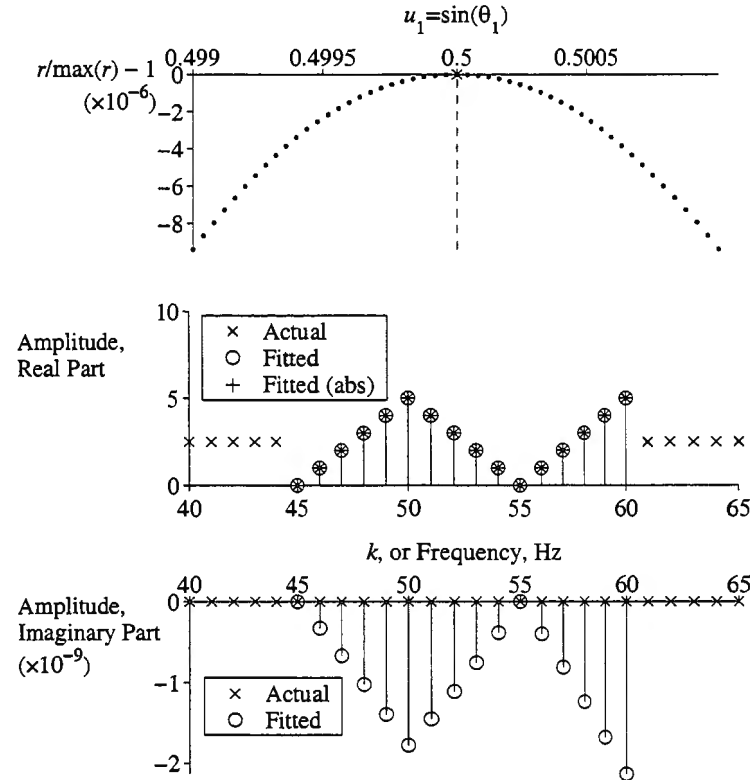


Figure 7. Results of Fitting with Source Components Outside the Fitting Band and Aligned with the Fitting Bins

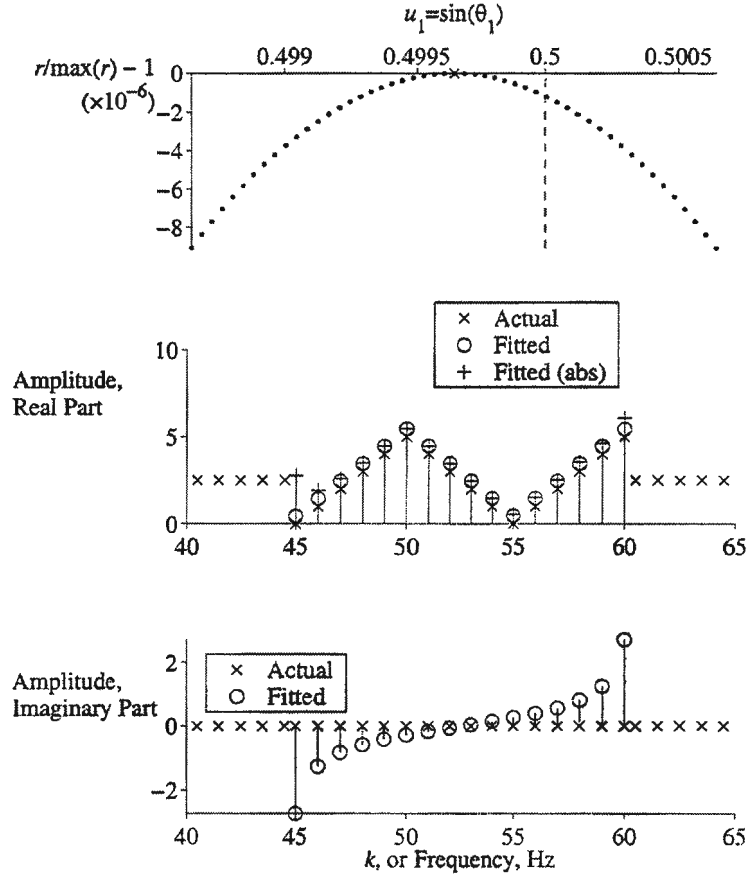


Figure 8. Results of Fitting with Source Components Outside the Fitting Band Misaligned, While Source Components Inside the Fitting Band Are Aligned with Fitting Bins

It is concluded from this set of numerical trials that the fitting procedure is able to accurately estimate the angle and amplitudes of a single multifrequency planewave, provided that the Fourier bin frequencies match the frequencies emitted by the source.

2.3.2 Comparison with Conventional Beamformer

In this section, the one-planewave fitting algorithm is compared to conventional beamforming. Consider the quantity $r(u_1)$ (equation (18)), which is maximized by the choice of arrival angle u_1 , and let the summand in equation (18) be denoted by $r(u_1, k)$; that is,

$$r(u_1) = \sum_{k=k_a}^{k_b} \left| \sum_{m=0}^{M-1} w_x(m) q(k, m) \exp \left[i \frac{2\pi k}{N} \beta(m) u_1 \right] \right|^2 \quad (37)$$

$$= \sum_{k=k_a}^{k_b} r(u_1, k), \quad (38)$$

where

$$r(u_1, k) = \left| \sum_{m=0}^{M-1} w_x(m) q(k, m) \exp \left[i \frac{2\pi k}{N} \beta(m) u_1 \right] \right|^2. \quad (39)$$

The conventional beamformer produces an output at frequency index k and arrival angle $u_1 = \sin(\theta_1)$ given by

$$P_c(u_1, k) = \frac{1}{N^2} \mathbf{v}'(k) \mathbf{R}(k) \mathbf{v}(k), \quad (40)$$

where $\mathbf{v}(k)$ is the M -element steering vector at frequency index k and at arrival angle θ_1 ,

$$\mathbf{v}(k) = \exp \left[i 2\pi \frac{f_1(k)}{c} \sin(\theta_1) x(m) \right] \quad (41)$$

$$= \exp \left[i \frac{2\pi k}{N} \beta(m) u_1 \right], \quad (42)$$

and the $M \times M$ sample covariance matrix $\mathbf{R}(k) = \mathbf{X}(k)\mathbf{X}'(k)$, where $\mathbf{X}(k)$ is the M -element vector of the Fourier coefficients at frequency k . If equation (40) is compared with equation (18), it is seen that, to within a scaling factor N , the conventional beamformer is equal to the summand of the function $r(u_1)$ with flat spatial weighting.

In the following examples, the “matched frequencies” case of the previous section is used; that is, the planewave is composed of frequencies corresponding to $k = f_k = 45:60$, and the arrival angle corresponds to $u_1 = 0.5$.

2.3.2.1 Noise-Free Case. Figure 9 shows the function $r(u_1, k)$ (equation (39)) on the left and the conventionally beamformed output (equation (40)) on the right. The darker regions denote high amplitude, and the lighter regions denote low amplitude. The set of input frequencies is shown as a set of white dots at $u_1 = 0.5$. The intensity image was produced using $10 \log r(u_1, k)$. For the conventional beamformer shown at the right, temporal FFTs with a length equal to the number of time samples for each sensor (1024 points) were used to estimate the covariance matrix. Both plots have the same k , u_1 , and gray intensity scales. As can be seen, the two plots are virtually identical.

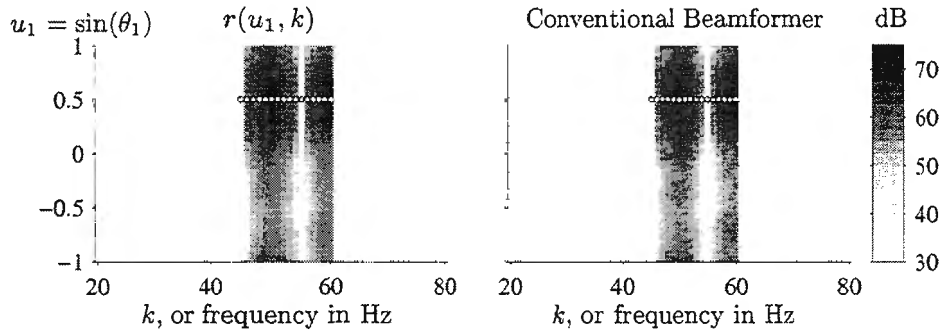


Figure 9. Comparison of Function $r(u_1, k)$ (Equation (39)) (Left) and Conventionally Beamformed Output (Right)

Figure 10 shows $r(u_1)$ and the sum over k of the conventional beamformer output, both plotted as functions of u_1 on a linear ordinate scale. The function $r(u_1)$ corresponds to the conventional beamformer output summed over the fitting frequencies. The resulting peak is at the correct value of u_1 ; namely, $u_1 = 0.5$. The two plots are identical and hence superimposed.

Figure 11 shows the strengths of the fitted frequency components and the amplitudes of the conventional beamformer output plotted against the frequency bin number at $u_1 = 0.5$. The top plot shows the actual strengths, and the bottom plot shows (1) the differences between the one-planewave fit and the input strengths (circles), and (2) the differences between the conventional beamformer output and the input strengths (triangles). There is a small error between the conventional beamformer output and the input strengths, which is not evident in the one-planewave fit.

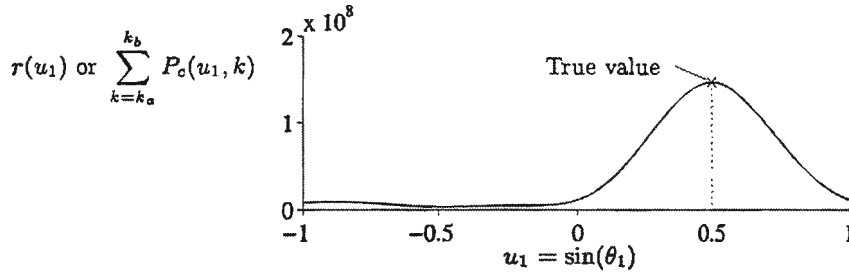


Figure 10. The Quantity $r(u_1)$ and the Sum over k of the Conventional Beamformer Output, Both Plotted as Functions of u_1

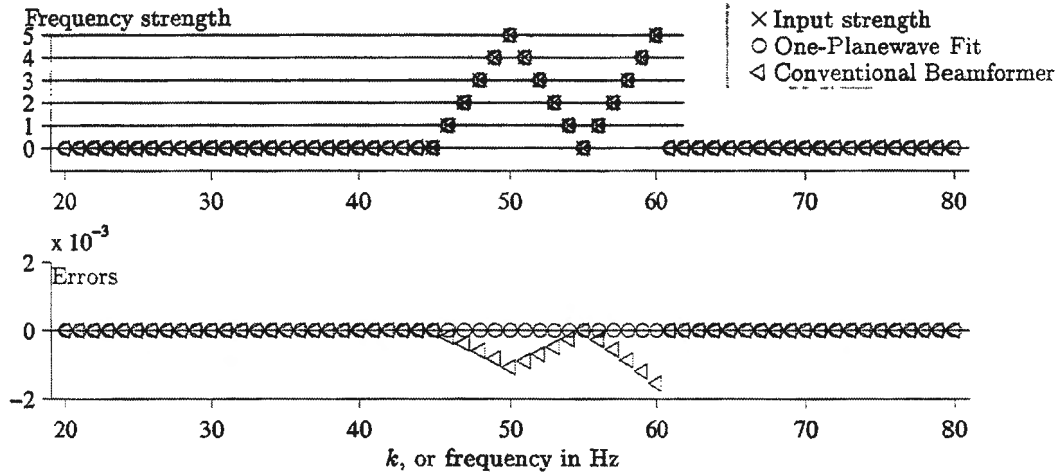


Figure 11. Strengths of the Fitted Frequency Components and the Amplitudes of the Conventional Beamformer Output Plotted Against Frequency Bin at $u_1 = 0.5$

2.3.2.2 Case with Noise. Complex normally-distributed random noise is added to the simulated pressure data in the following manner:

```
snr = -10;
Noise = randn(size(pnm)) + i*randn(size(pnm));
As = mean(std(pnm));
An = mean(std(Noise));
NoiseScaleFactor = As / (An*10^(snr/20));
pnm = pnm + Noise * NoiseScaleFactor;
```

The quantity snr defines the desired signal-to-noise ratio, which is equal to -10 dB in this case. The matrix Noise is the same size as the data matrix and has independent real and imaginary parts. The quantity $\text{std}(\text{pnm})$ is an M -element vector of standard deviations—one for each array element. The quantity A_s is the mean of these standard deviations; a similar measure is made for the noise amplitude A_n . The noise matrix is multiplied by the scalar NoiseScaleFactor to obtain the desired SNR, and this quantity is added to the data sample matrix.

Figure 12 shows the function $r(u_1, k)$ (equation (39)) on the left and the conventionally beamformed output (equation (40)) on the right for this case, with an SNR of -10 dB. For the conventional beamformer shown on the right, temporal FFTs with a length equal to the number of time samples for each sensor (1024 points) were used to estimate the covariance matrix. The two plots are very similar. Further similarities between the one-planewave fitting algorithm and conventional beamforming are identified below.

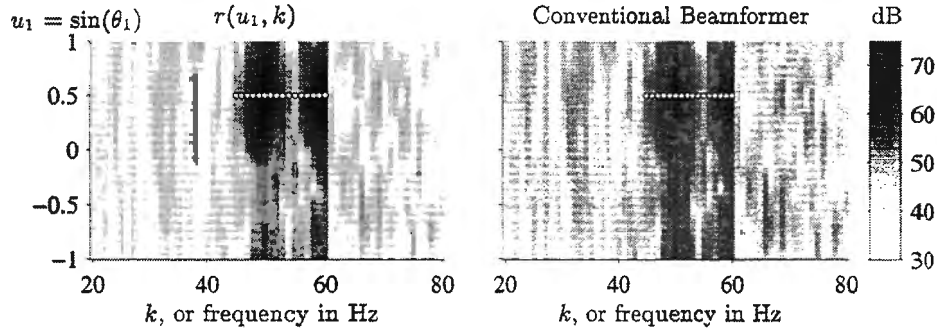


Figure 12. The Function $r(u_1, k)$ (Equation (39)) (left) and the Conventionally Beamformed Output (Equation (40)) (right) for SNR of -10 dB

Figure 13 displays $r(u_1)$ and the sum over k of the conventional beamformer output, both plotted as functions of u_1 on a linear ordinate scale. The two lines are, as previously shown, virtually identical.

Figure 14 shows the frequency strengths plotted against the frequency bin number at $u_1 = 0.5$. As seen earlier in the noise-free case, there is no significant difference between the one-planewave fit (dots) and the conventional beamformer (triangles).

Figure 15 compares the outputs of the conventional beamformer and the one-planewave fit for the range of input SNRs shown at the left of each row of plots. Ten realizations are shown for each SNR value. The axis scale for each column is shown at the bottom and is constant within each column, except for the second one. The first column shows the conventional beamformer output plotted as a surface in decibels; the gray scale values are indicated to the left of the top plot and are constant throughout column 1. The

input frequencies are shown as the white dots, and the peak value of the beamformer output is shown by the white cross in each plot. Column 2 shows $r(u_1)$ and the sum over k of the conventional beamformer output, both plotted as functions of u_1 on a linear ordinate scale. Solid lines in this column are the one-planewave fits; broken lines show the sum over k of the conventional beamformer outputs, but these are superimposed on the solid lines and are hence invisible. Column 3 shows the frequency strengths for the one-planewave fit (circles) and the conventional beamformer (triangles) at $u_1 = 0.5$. The set of amplitudes listed in table 1 on page 12 was used. There is no significant difference between the outputs of the one-planewave fit and the conventional beamformer.

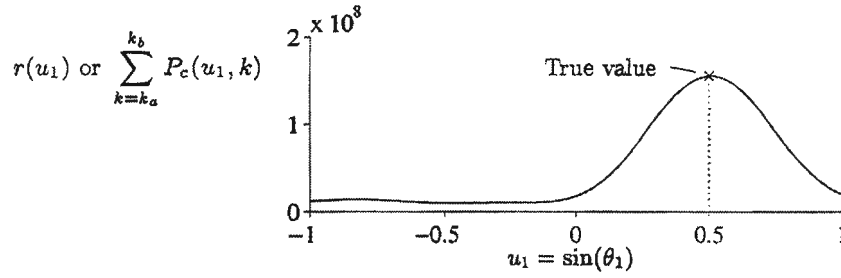


Figure 13. The Quantity $r(u_1)$ and the Sum over k of the Conventional Beamformer Output, Both Plotted as Functions of u_1

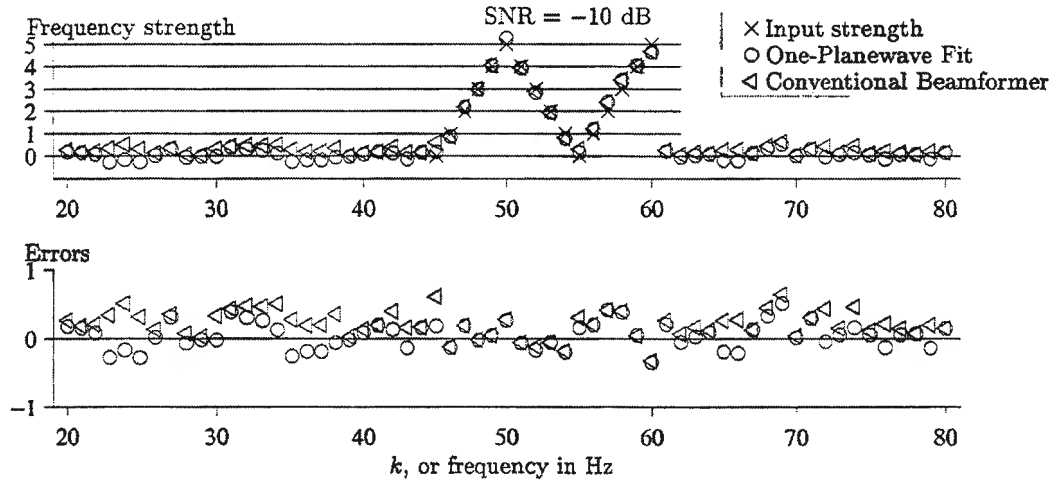


Figure 14. Frequency Strengths Plotted Against Frequency Bin Number at $u_1 = 0.5$ for the Case with Noise

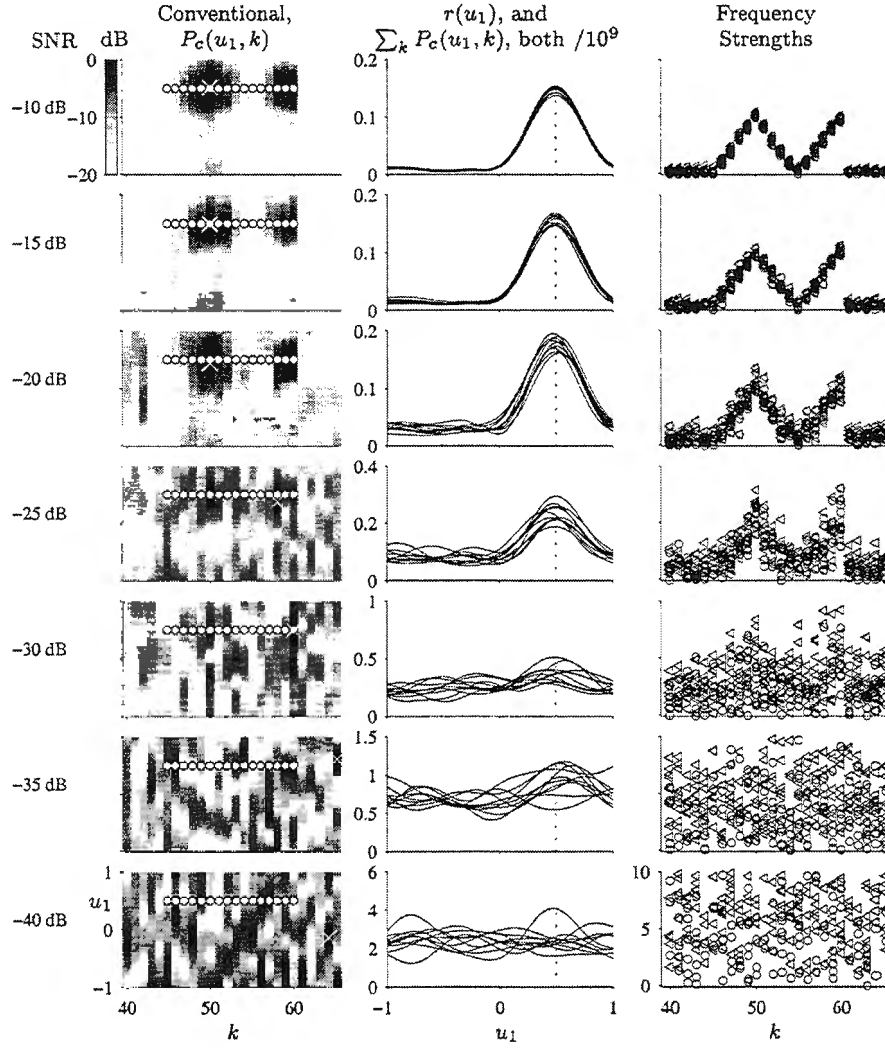


Figure 15. Conventional Beamformer Output and the One-Planewave Fit Output for Various Signal-To-Noise Ratios

3. TWO-PLANEWAVE FIT FOR UNEQUALLY-SPACED LINE ARRAYS

3.1 THEORY

The discrete data available are again $\{p(n, m)\}$ for $n = 0:N-1$ and $m = 0:M-1$, and the fitting frequencies are taken as

$$f_k = \frac{k}{T} = \frac{k}{N\Delta} \quad \text{for } k = k_a : k_b. \quad (43)$$

The range (k_a, k_b) represents the common frequencies for the two planewave fits. (It is possible to generalize to the case where only some of the fitting frequencies $\{f_k\}$ are common to the two planewaves; the corresponding complex amplitudes $\{a_1(k)\}$ and $\{a_2(k)\}$ would then be set to zero in the appropriate nonoverlapping frequency bins.) Also defined are

$$\alpha_k \equiv \frac{2\pi k}{N}, \quad \beta(m) \equiv \frac{x(m)}{c\Delta} \quad \text{for } m = 0:M-1. \quad (44)$$

If two planewaves arrive from hypothesized angles u_1 and u_2 , the observed complex pressure field over observation interval $T = N\Delta$ is modeled as

$$\tilde{p}_2(t, x) \equiv \sum_{k=k_a}^{k_b} a_1(k) \exp\left[i2\pi \frac{k}{T} \left(t - \frac{x}{c} u_1\right)\right] + \sum_{k=k_a}^{k_b} a_2(k) \exp\left[i2\pi \frac{k}{T} \left(t - \frac{x}{c} u_2\right)\right], \quad (45)$$

where the hypothesized amplitudes $\{a_1(k)\}$ and $\{a_2(k)\}$ are complex. The two (broadband) sources are assumed to be uncorrelated with each other (see section 4 for a correlated case). Therefore, the sampled pressure field is modeled as

$$\begin{aligned} \tilde{p}_2(n\Delta, x(m)) &= \sum_{k=k_a}^{k_b} a_1(k) \exp\left[i\alpha_k(n - \beta(m)u_1)\right] \\ &\quad + \sum_{k=k_a}^{k_b} a_2(k) \exp\left[i\alpha_k(n - \beta(m)u_2)\right]. \end{aligned} \quad (46)$$

A total average squared error between the actual received data and the model (equation (46)) is defined as

$$e = \frac{1}{N} \sum_{n=0}^{N-1} \sum_{m=0}^{M-1} w_x(m) \left| \tilde{p}(n\Delta, x(m)) - \tilde{p}_2(n\Delta, x(m)) \right|^2, \quad (47)$$

where a flat temporal weighting $w_t(n) = 1/N$ for $n = 0:N-1$ is used, and a spatial error-weighting function $w_x(m)$, which is real and positive, is allowed. Then the error e can be expressed in the form

$$\begin{aligned} e &= \frac{1}{N} \sum_{n,m} w_x(m) \left| p(n, m) - \sum_{k=k_a}^{k_b} a_1(k) \exp\left[i\alpha_k(n - \beta(m)u_1)\right] \right. \\ &\quad \left. - \sum_{k=k_a}^{k_b} a_2(k) \exp\left[i\alpha_k(n - \beta(m)u_2)\right] \right|^2 \end{aligned} \quad (48)$$

$$\equiv \frac{1}{N} \sum_{n,m} w_x(m) |d(n, m)|^2 = \sum_m w_x(m) \frac{1}{N} \sum_n |d(n, m)|^2. \quad (49)$$

Letting

$$D(l, m) = \sum_{n=0}^{N-1} \exp(-i2\pi nl/N) d(n, m) \quad \text{for } l = 0:N-1, \quad (50)$$

then

$$\begin{aligned} \frac{1}{N^2} \sum_{l=0}^{N-1} |D(l, m)|^2 &= \frac{1}{N^2} \sum_{l=0}^{N-1} \sum_{n, \underline{n}} \exp \left[-i2\pi(n - \underline{n}) \frac{l}{N} \right] d(n, m) d^*(\underline{n}, m) \\ &= \frac{1}{N} \sum_{n=0}^{N-1} |d(n, m)|^2, \end{aligned} \quad (51)$$

which is a discrete form of Parseval's Theorem. The error e follows from equation (49) as

$$e = \sum_m w_x(m) \frac{1}{N^2} \sum_l |D(l, m)|^2. \quad (52)$$

However, from equations (49), (50) and (44),

$$\begin{aligned} \frac{1}{N} D(l, m) &= \frac{1}{N} \sum_n \exp(-i2\pi nl/N) \left\{ p(n, m) \right. \\ &\quad \left. - \sum_k a_1(k) \exp[i\alpha_k(n - \beta(m)u_1)] - \sum_k a_2(k) \exp[i\alpha_k(n - \beta(m)u_2)] \right\} \\ &= q(l, m) - a_1(l) \exp[-i\alpha_l \beta(m)u_1] - a_2(l) \exp[-i\alpha_l \beta(m)u_2], \end{aligned} \quad (53)$$

where the temporal discrete Fourier transforms have been defined as

$$q(l, m) = \frac{1}{N} \sum_{n=0}^{N-1} \exp(-i2\pi nl/N) p(n, m), \quad (54)$$

for $l = 0:N-1$, $m = 0:M-1$. Therefore, equation (52) becomes

$$\begin{aligned} e &= \sum_m w_x(m) \sum_l \left| q(l, m) - a_1(l) \exp[-i\alpha_l \beta(m)u_1] \right. \\ &\quad \left. - a_2(l) \exp[-i\alpha_l \beta(m)u_2] \right|^2. \end{aligned} \quad (55)$$

To minimize e , consider

$$\begin{aligned} \frac{\partial e}{\partial a_1^*(k)} &= - \sum_m w_x(m) \left\{ q(k, m) - a_1(k) \exp[-i\alpha_k \beta(m)u_1] \right. \\ &\quad \left. - a_2(k) \exp[-i\alpha_k \beta(m)u_2] \right\} \exp[i\alpha_k \beta(m)u_1] \\ &= - \sum_m w_x(m) q(k, m) \exp[i\alpha_k \beta(m)u_1] + a_1(k) \sum_m w_x(m) \\ &\quad + a_2(k) \sum_m w_x(m) \exp[i\alpha_k \beta(m)(u_1 - u_2)] \\ &= -X(k, \alpha_k u_1) + a_1(k) + a_2(k) W_x(\alpha_k(u_1 - u_2)) \quad \text{for } k = k_a : k_b, \end{aligned} \quad (56)$$

where

$$X(k, \gamma) \equiv \sum_m w_x(m) q(k, m) \exp[i\gamma\beta(m)] \quad \text{for } k = k_a : k_b, \text{ all } \gamma, \quad (57)$$

$$W_x(\gamma) \equiv \sum_m w_x(m) \exp[i\gamma\beta(m)] \quad \text{for all } \gamma, \quad (58)$$

and $W_x(0) = \sum_m w_x(m) = 1$ is used. Similarly,

$$\frac{\partial e}{\partial a_2^*(k)} = -X(k, \alpha_k u_2) + a_1(k) W_x^*(\alpha_k(u_1 - u_2)) + a_2(k) \quad (59)$$

for $k = k_a : k_b$. Minimization of error e results in simultaneous equations for the conditionally best-fitting coefficients $\{a_1(k)\}$ and $\{a_2(k)\}$, namely,

$$\left. \begin{aligned} a_1(k) + W_k a_2(k) &= X(k, \alpha_k u_1) \\ W_k^* a_1(k) + a_2(k) &= X(k, \alpha_k u_2) \end{aligned} \right\} \text{for } k = k_a : k_b, \quad (60)$$

and $W_k \equiv W_x(\alpha_k(u_1 - u_2))$. The solutions for the conditionally optimal complex amplitudes are, for $k = k_a : k_b$,

$$\begin{aligned} a_1(k) &= \frac{X(k, \alpha_k u_1) - W_k X(k, \alpha_k u_2)}{1 - |W_k|^2}, \\ a_2(k) &= \frac{X(k, \alpha_k u_2) - W_k^* X(k, \alpha_k u_1)}{1 - |W_k|^2}. \end{aligned} \quad (61)$$

Decoupling in frequency index k is due to the flat temporal weighting $\{w_t(n)\}$ and to the fact that frequency increment $\Delta f = 1/T$. The conditionally minimal value of e is now, from equation (55),

$$\begin{aligned} \underline{e} &= \sum_m w_x(m) \sum_k \left\{ q(k, m) - a_1(k) \exp[-i\alpha_k\beta(m)u_1] \right. \\ &\quad \left. - a_2(k) \exp[-i\alpha_k\beta(m)u_2] \right\} q^*(k, m) \\ &= \sum_{m,k} w_x(m) |q(k, m)|^2 - \sum_k a_1(k) X^*(k, \alpha_k u_1) - \sum_k a_2(k) X^*(k, \alpha_k u_2) \\ &= \sum_{m,k} w_x(m) |q(k, m)|^2 - r(u_1, u_2), \end{aligned} \quad (62)$$

where the solutions for $a_1(k)$ and $a_2(k)$ from equation (61) have been used, as well as the fact that the initial double sum over m and k is independent of u_1 and u_2 , and

$$r(u_1, u_2) = \sum_{k=k_a}^{k_b} \frac{|X(k, \frac{2\pi k}{N} u_1)|^2 + |X(k, \frac{2\pi k}{N} u_2)|^2 - 2\Re\left\{W_x\left(\frac{2\pi k}{N}(u_1 - u_2)\right)X^*\left(k, \frac{2\pi k}{N} u_1\right)X\left(k, \frac{2\pi k}{N} u_2\right)\right\}}{1 - \left|W_x\left(\frac{2\pi k}{N}(u_1 - u_2)\right)\right|^2}, \quad (63)$$

where \Re denotes the real part, and, from equations 57, 58, and 54,

$$X(k, \frac{2\pi k}{N}u) = \sum_{m=0}^{M-1} w_x(m) q(k, m) \exp \left[i \frac{2\pi k}{N} \frac{x(m)}{c\Delta} u \right], \quad (64)$$

$$W_x(\frac{2\pi k}{N}u) = \sum_{m=0}^{M-1} w_x(m) \exp \left[i \frac{2\pi k}{N} \frac{x(m)}{c\Delta} u \right], \quad (W_x(0) = 1), \quad (65)$$

$$q(k, m) = \frac{1}{N} \sum_{n=0}^{N-1} p(n, m) \exp(-i2\pi kn/N) \quad \text{for } m = 0:M-1 \quad (66)$$

for $k = 0:N-1$. However, only the values for $k = k_a:k_b$ are needed in equation (63). Equation (66) consists of M N -point temporal discrete Fourier transforms.

To further minimize the conditional error \underline{e} in equation (62), the quantity $r(u_1, u_2)$ given by equation (63) must be maximized by choice of both arrival angles u_1 and u_2 , which may be taken as $u_1 < u_2$ without loss of generality. The location of the maximum of $r(u_1, u_2)$ is denoted by \hat{u}_1, \hat{u}_2 .

The factor $\frac{2\pi k}{N} \frac{x(m)}{c\Delta} u$ in equation (64) is exactly the phase compensation required at frequency $\frac{k}{N\Delta}$ and array element m , to coherently “line up” all components arriving at angle u ($u = 0$ is broadside). Thus, equation (64) is a “coherent” sum carried out prior to the “incoherent” sum over k (frequency) in equation (63). The sum for spatial window W_x in equation (65) cannot be carried out *a priori* in closed form because of the irregular element locations $\{x(m)\}$; also, $W_x(\gamma)$ is complex and will remain so for general $\{x(m)\}$ locations.

From equation 63, it is noted that for given u_1, u_2 , and k , only three complex quantities need to be computed. However, they must be combined according to equation (63), yielding a purely real quantity, which is then summed over the frequency band of interest, $k = k_a:k_b$. Equations (64) and (65) cannot be carried out with the FFT because the element locations $\{x(m)\}$ are unevenly spaced.

A measure of the total power in arrival 1 is available, by reference to equation (45), as

$$P_1 = \sum_{k=k_a}^{k_b} |\hat{a}_1(k)|^2, \quad (67)$$

where $\{\hat{a}_1(k)\}$ are the optimal coefficients obtained from equation (61), using angle values \hat{u}_1 and \hat{u}_2 , after the best angles (namely, \hat{u}_1 and \hat{u}_2) have been determined from the maximization of $r(u_1, u_2)$ given by equation (63). If P_1 is large, then source 1 could be coherently subtracted from the input data $p(n, m)$, as indicated in equation (48). If P_1 is small, then the coefficients $\{\hat{a}_1(k)\}$ could be discarded and considered as noise.

With the conditionally optimal coefficients $\{a_1(k)\}$ and $\{a_2(k)\}$ for specified u_1 and u_2 , the conditionally minimal time-space residual is, using equation (46),

$$\begin{aligned} \underline{p}(n, m) &\equiv \tilde{p}(n\Delta, x(m)) - \tilde{p}_2(n\Delta, x(m)) \\ &= p(n, m) - \sum_k a_1(k) \exp \left[i \frac{2\pi k}{N} (n - \beta(m)u_1) \right] \\ &\quad - \sum_k a_2(k) \exp \left[i \frac{2\pi k}{N} (n - \beta(m)u_2) \right]. \end{aligned} \quad (68)$$

The unconditionally minimal time-space residual is

$$\begin{aligned}\hat{p}(n, m) = p(n, m) - \sum_k \hat{a}_1(k) \exp \left[i \frac{2\pi k}{N} (n - \beta(m) \hat{u}_1) \right] \\ - \sum_k \hat{a}_2(k) \exp \left[i \frac{2\pi k}{N} (n - \beta(m) \hat{u}_2) \right]\end{aligned}\quad (69)$$

for $n = 0:N-1$, $m = 0:M-1$. The corresponding unconditionally minimal residual in the frequency-space domain is, using equation (66),

$$\begin{aligned}\hat{q}(k, m) = q(k, m) - \hat{a}_1(k) \exp \left[-i \frac{2\pi k}{N} \beta(m) \hat{u}_1 \right] \\ - \hat{a}_2(k) \exp \left[-i \frac{2\pi k}{N} \beta(m) \hat{u}_2 \right] \quad \text{for } k = k_a:k_b, m = 0:M-1.\end{aligned}\quad (70)$$

These residuals are devoid of the two strongest planewave arrivals and can now be processed further to detect additional (weak) arrivals. Without this coherent subtraction, the two strong arrivals could override a weak arrival in close angular proximity.

3.2 IMPLEMENTATION

The first step of the two-planewave fit is to find the pair of values, \hat{u}_1 and \hat{u}_2 , that maximize the function $r(u_1, u_2)$ given by equation (63). Three-dimensional arrays are used to store the quantities $X(k, 2\pi k u_1/N)$, $X(k, 2\pi k u_2/N)$, and $W_x(2\pi k (u_1 - u_2)/N)$, each being considered as a function of u_1 , u_2 , and k . The array geometry, sampling interval, planewave amplitudes and directions, etc., are defined as follows:

```
f1_source = 45:60;
a1 = [0 1 2 3 4 5 4 3 2 1 0 1 2 3 4 5];
ka = 45;
kb = 60;
f2_source = 45:60;
a2 = 5 - a1;
u1_source = 0; % sin(source angle)
u2_source = .5; % sin(source angle)
i = sqrt(-1);
N = 1024; % Number of time points
delta = 1/1024; % sampling increment (s)
c = 1500; % sound speed (m/s)
tvect = 0:delta:(N - 1)*delta; % vector of sample times
xarray = linspace(0,50,11).';
M = length(xarray); % Number of sensors
wx_m = ones(1,M)/M; % spatial error weighting
```

The time-space data are generated by summing the frequency components of the two sources:

```
[xmatrix,tmatrix] = meshgrid(xarray,tvect);
pnm = zeros(N,M);
arg1 = tmatrix - xmatrix*u1_source/c;
```

```

arg2 = tmatrix - xmatrix*u2_source/c;
K = length(f1_source);
for k = 1:K
    pnm = pnm + a1(k)*exp(2*pi*f1_source(k)*arg1*i) + ...
        a2(k)*exp(2*pi*f2_source(k)*arg2*i);
end

```

The Fourier transform $q(k, m)$ given by equation (66) (an $M \times K$ matrix) and the phase factor $\phi = 2\pi k x(m)/(Nc\Delta)$ (also $M \times K$) used in equations (64) and (65) are calculated as follows:

```

% Calculate Fourier transform and phase matrix for use in the
% calculation of r:
k_vt = ka:kb;
n_vt = 0:N-1;
[k_mx, n_mx] = meshgrid(k_vt, n_vt);
E = exp((-2*pi*k_mx.*n_mx/N)*i);
% Fourier transform: sum over n done with matrix product:
q = (1/N)*pnm.'*E;
% Phase factor used in argument of exponential
% in calculation of X and W:
phi = 2*pi*xarray*k_vt/(N*c*delta);

```

The vector `xarray` is of size $M \times 1$, and the vector `k_vt` is of size $1 \times K$. The quantity $W_x(2\pi k(u_1 - u_2)/N)$ is calculated using two nested for-loops and stored in an $N_u \times N_u \times K$ array, while an intermediate array `Xku` stores values of $X(k, 2\pi k u/N)$ in a $K \times N_u$ array, where $u = -1 + \delta_u[0:(N_u - 1)]$, $\delta_u = 2/(N_u - 1)$, and N_u is the number of values used to span the range of u :

```

Nuspan = 40;
u_span = linspace(-1, 1, Nuspan);
Xku = zeros(K, Nuspan);
Wkuu = zeros(Nuspan, Nuspan, K);
iu2 = 0;
for this_u2 = u_span
    iu2 = iu2 + 1;
    % Matrix product does sum over m:
    Xku(:, iu2) = (wx_m*(q.*exp(phi*this_u2*i))).';
    iu1 = 0;
    for this_u1 = u_span
        iu1 = iu1 + 1;
        Emkuu = exp(phi*(this_u1 - this_u2)*i);
        % Matrix product does sum over m:
        Wkuu(iu2, iu1, :) = wx_m*Emkuu;
    end
end
end

```

The $K \times N_u$ array `Xku` is now copied into two (three-dimensional) arrays that have the same dimensions as `Wkuu`. These dimensions correspond to u_1 varying across the columns and u_2 varying down the rows. In all cases, k varies along the third dimension. This copying is carried out as follows:

```
Xku1 = permute( repmat(Xku,[1 1 Nuspan]),[3,2,1]);
Xku2 = permute( repmat(Xku,[1 1 Nuspan]),[2,3,1]);
```

The matrices W_{kuu} , X_{ku1} , and X_{ku2} are now used to compute the addend in equation (63), with the result summed over k , corresponding to dimension number 3:

```
top = abs(Xku1).^2 + abs(Xku2).^2 ...
      - 2*real(Wkuu.*conj(Xku1).*Xku2);
bot = 1 - abs(Wkuu).^2;
ru1u2 = sum(top./bot,3); % sum over the third index, which is k
```

The matrix $ru1u2$ is of size $N_u \times N_u$. The location of the maximum value of this matrix gives an initial estimate of \hat{u}_1 and \hat{u}_2 , as follows:

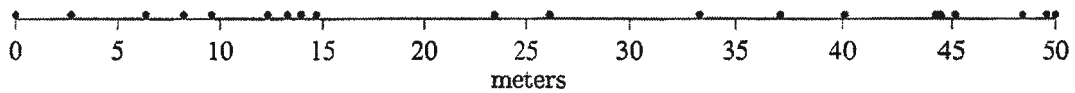
```
[dum,jmax] = max(max(ru1u2));
[dum,imax] = max(ru1u2(:,jmax));
hatu1 = u_span(jmax);
hatu2 = u_span(imax);
```

Figure 16 shows calculations of the quantity $r(u_1, u_2)$ for different values of the actual source angles u_{s1} and u_{s2} . Contours are plotted at the set of values shown at the top right of the plots, with the actual source angles u_{s1} and u_{s2} indicated by the white dot in each plot. The function $r(u_1, u_2)$ is symmetric under exchange of u_1 and u_2 , as expected by equation (63). Equation (63) is undefined at $u_1 = u_2$; therefore, calculating $r(u_1, u_2)$ for $u_1 = u_2$ has been avoided. (See the appendix for an alternative formulation without this singularity.) For the cases where the source angles were equal (plots at the top and right edge of the figure), the $r(u_1, u_2)$ surfaces have no unique maxima and correspond to a single planewave source.

Initial estimates of \hat{u}_{01} and \hat{u}_{02} were obtained by finding the location of the peak of $ru1u2$; now those estimates will be refined using the iterative procedure `fminsearch`, and the function `calcru1u2`, which returns a scalar $r(u_1, u_2)$ for a given input vector $[u_1, u_2]$.

3.3 EXAMPLE OF NOISE-FREE SIMULATIONS

The sketch below shows a noise-free simulation that was run for an array of 20 randomly distributed sensors placed in a line at the following positions (meters): 0, 2.7149, 6.3877, 8.2533, 9.5938, 12.3172, 13.2960, 13.9596, 14.6925, 23.4220, 26.1543, 33.2634, 37.1476, 40.0923, 44.2354, 44.4607, 45.1650, 48.3877, 49.5603, and 50.



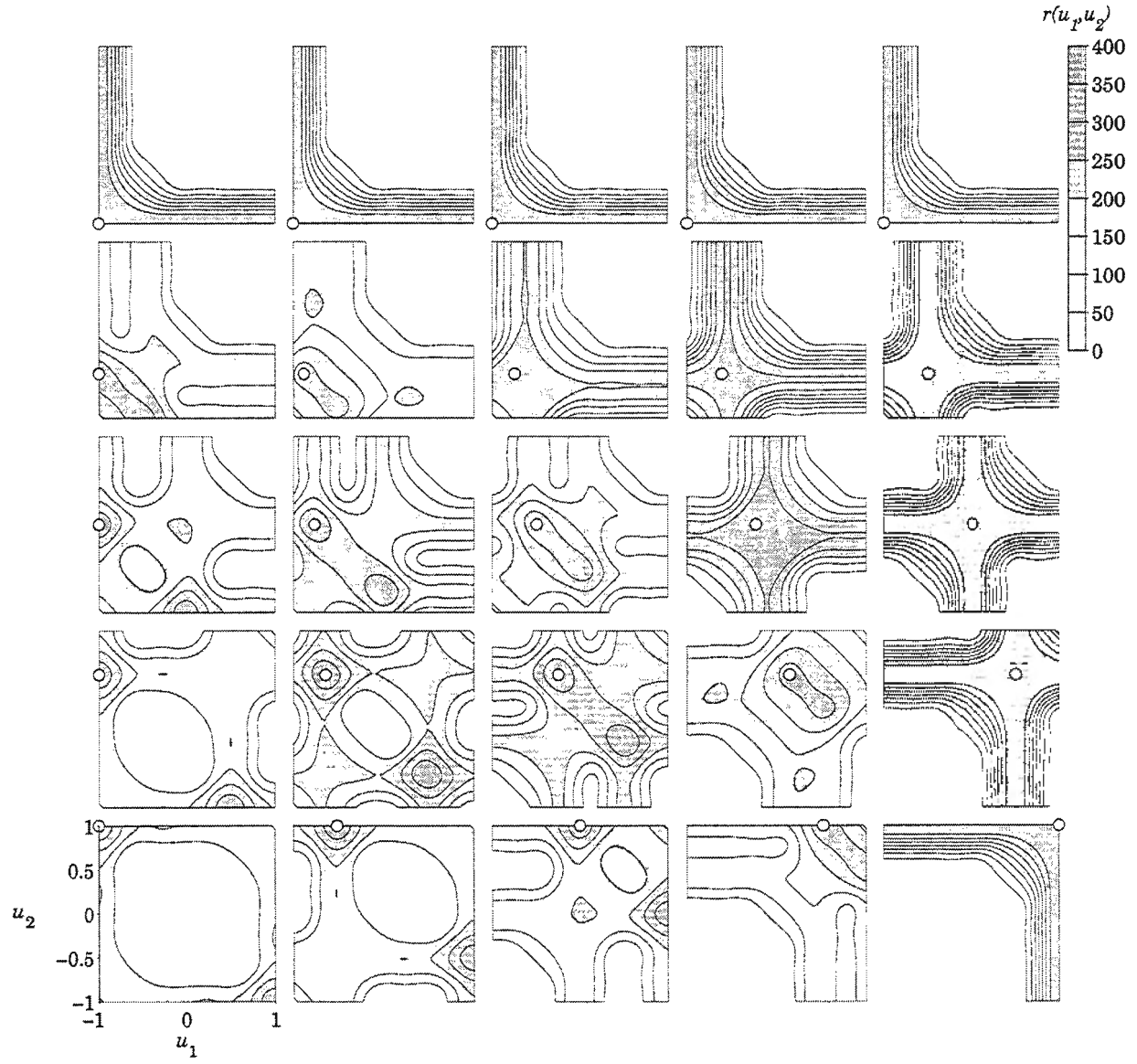


Figure 16. Quantity $r(u_1, u_2)$ for Different Values of Source Angles u_{s1} and u_{s2}

Two sources were simulated, one at $u_{s1} = -0.01$, and the other at $u_{s2} = +0.01$, i.e., 0.57° either side of broadside. Both emitted a set of planewaves at frequencies between 45 and 60 Hz, with a spacing of 1 Hz. The amplitudes of the planewaves are as shown in figure 17.

Figure 18 shows contours of the quantity $r(u_1, u_2)$. The plot on the left shows r for all possible values of u_1 and u_2 , and the plot on the right presents a magnified view of a small region around the true angles of the sources. The angles found by the search procedure are indicated on the magnified plot, with the point corresponding to these angles laying on a very shallow hyperbolically (banana-) shaped ridge that asymptotically approaches the lines $u_1 = 0$ and $u_2 = 0$. The entire surface is symmetric under exchange of u_1 and u_2 , as expected.

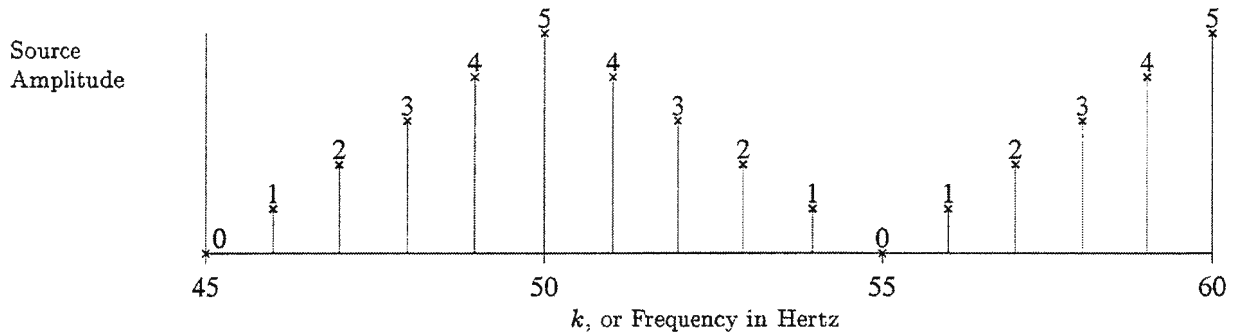


Figure 17. Amplitudes of the Two Planewaves Used for the Two-Planewave Fit

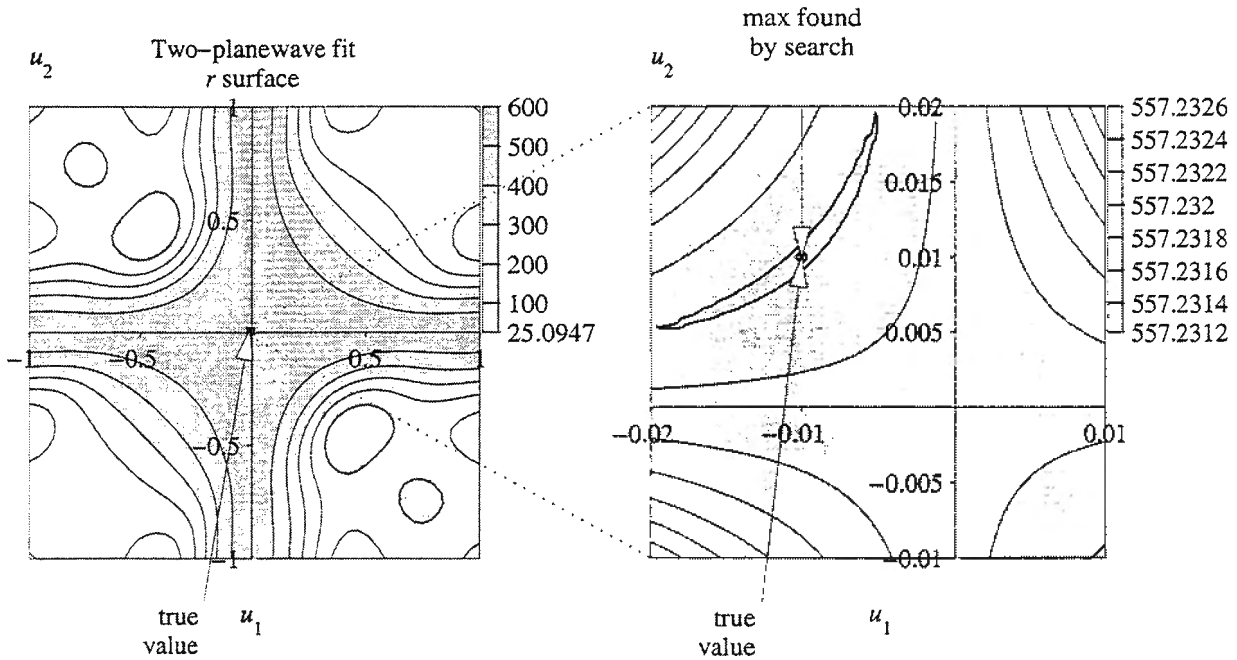


Figure 18. Quantity $r(u_1, u_2)$ for the Two-Planewave Fit

The previous result is compared with conventional beamforming results in figure 19. The top plot provides contours of the same two-planewave fit that was shown in the previous plot, together with the zoomed-in region to the right, close to the true source values. The conventionally beamformed result is shown in the lower-left plot, with a zoomed-in version to the right, surrounding the true source angles -0.01 and $+0.01$. The conventional beamformer output was found for a frequency of 50 Hz, which was one of the frequencies corresponding to the largest amplitude emitted by the sources (see the source amplitude plot in figure 17). There is no evidence at all of the angles corresponding to the two sources in the conventionally beamformed result.

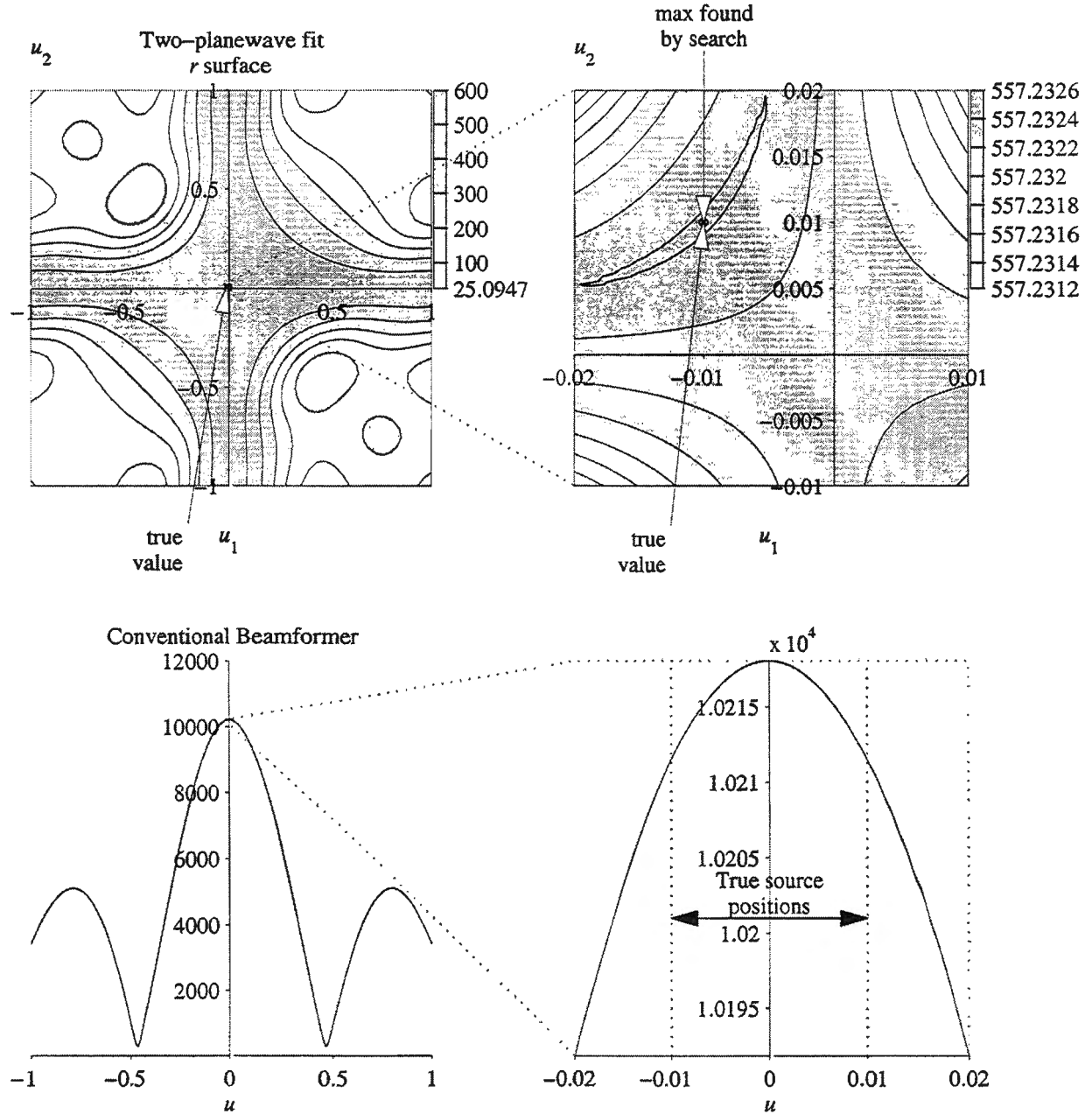


Figure 19. The $r(u_1, u_2)$ Surface Compared to Conventionally Beamformed Results

Figure 20 shows the same comparison, but this time, the sources have been more widely separated in angle, corresponding to $u_{s1}, u_{s2} = \pm 0.1715$. These values were found by adjusting the angular separation until a double peak began to be observed in the conventional beamformer output. The lower-right plot shows that even though the conventional beamformer was able to produce a double peak in this instance, the peaks did not occur at the correct values of u , which are indicated by the broken lines.

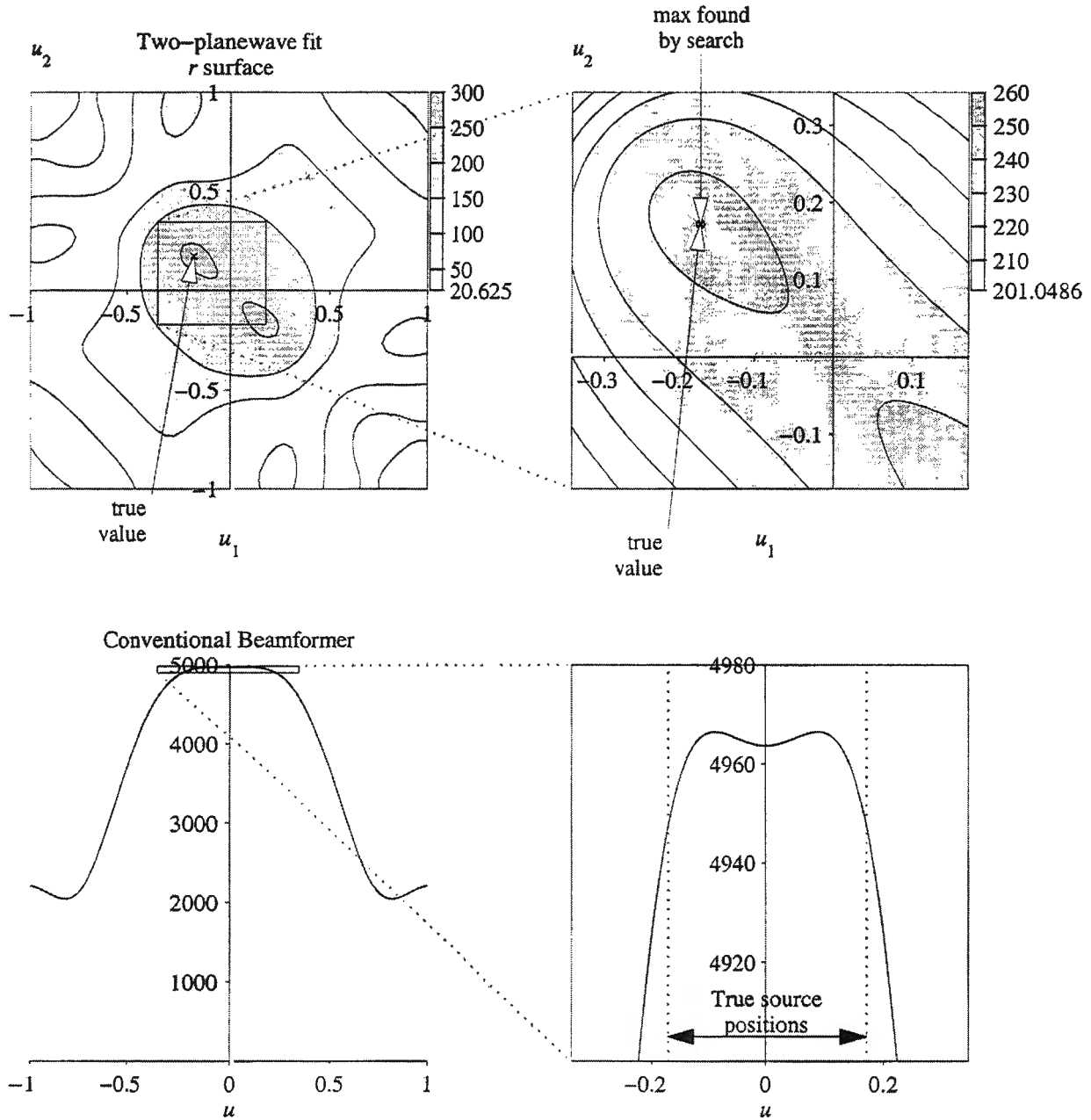


Figure 20. The $r(u_1, u_2)$ Surface Compared to Conventionally Beamformed Results for Separated Sources

Figure 21 shows the results for very widely separated sources and for a single source. Case (a) illustrates the presence of two sources (at $u_{s1}, u_{s2} = \pm 0.75$) and case (b) illustrates the presence of only one source (at $u_{s1} = -0.75$). The top plots are the two two-planewave fits, and the bottom plots are the conventionally beamformed results. The two-planewave fit ((a) top) was able to accurately determine the angles corresponding to the two planewaves. Although the conventional beamformer ((a) bottom) shows two distinct peaks, the mutual interference between the two planewaves gave rise to peaks that were closer together in angle than the true sources. The same conventional beamformer was able to accurately determine the direction of the single planewave ((b) bottom).

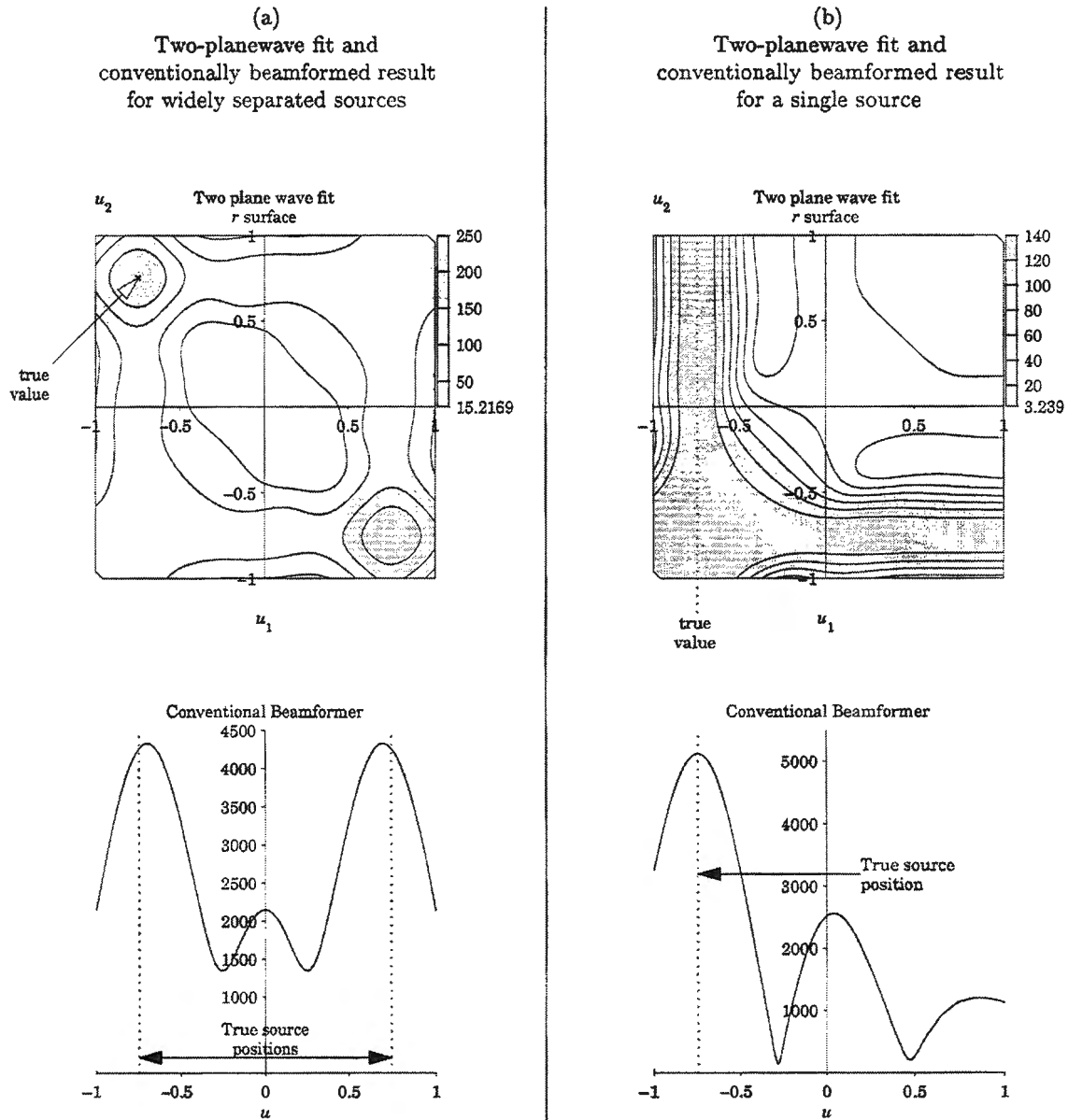


Figure 21. Two-Planewave Fits and Conventional Beamforming Outputs for (a) Two Widely Separated Sources and (b) A Single Source

4. TWO-PLANEWAVE FIT TO MULTIPATH ARRIVALS FOR UNEQUALLY SPACED LINE ARRAYS

The discrete data available are $\{p(n, m)\}$ for $n = 0:N-1$ and $m = 0:M-1$. Here, $p(n, m) = \tilde{p}(n\Delta, x(m))$, where $\tilde{p}(t, x)$ is the continuous received pressure field at time t and location x , while Δ is the time-sampling increment and $\{x(m)\}$ are the sensor positions.

A planewave arriving from angle $u_1 = \sin \theta_1$ is modeled according to the following summation:

$$\tilde{p}_1(t, x) = \sum_{k=k_a}^{k_b} a_1(k) \exp \left[i2\pi \frac{k}{T} \left(t - \frac{x}{c} u_1 \right) \right]. \quad (71)$$

A multipath arrival with relative gain G and delay τ from arrival angle u_2 is modeled as

$$\tilde{p}_1(t, x) = G \sum_{k=k_a}^{k_b} a_1(k) \exp \left[i2\pi \frac{k}{T} \left(t - \tau - \frac{x}{c} u_2 \right) \right], \quad (72)$$

where the *same* set of complex amplitudes $\{a_1(k)\}$ is utilized. Gain G is real and independent of frequency in the band of interest. As a result, the modeled samples at times $\{n\Delta\}$ and locations $\{x(m)\}$ comprise a two-planewave fit:

$$\tilde{p}_2(n\Delta, x(m)) \equiv \sum_k a_1(k) \exp \left[i2\pi \frac{k}{T} n\Delta \right] \left\{ \exp \left[-i2\pi \frac{k}{T} \frac{x(m)}{c} u_1 \right] \right. \quad (73)$$

$$\left. + G \exp \left[-i2\pi \frac{k}{T} \tau - i2\pi \frac{k}{T} \frac{x(m)}{c} u_2 \right] \right\}. \quad (74)$$

The dimensionless parameters are defined as

$$\alpha_k \equiv \frac{2\pi k}{N}, \quad \beta(m) \equiv \frac{x(m)}{c\Delta}, \quad \lambda \equiv \frac{\tau}{\Delta}. \quad (75)$$

The modeled data samples can then be written as

$$\tilde{p}_2(n\Delta, x(m)) = \sum_k a_1(k) \exp(i\alpha_k n) \left\{ \exp[-i\alpha_k \beta(m) u_1] + G \exp[-i\alpha_k \lambda - i\alpha_k \beta(m) u_2] \right\}. \quad (76)$$

An average squared error between the data and the fit (equation (76)) is defined as

$$e = \frac{1}{N} \sum_{n,m} w_x(m) \left| \tilde{p}(n\Delta, x(m)) - \tilde{p}_2(n\Delta, x(m)) \right|^2, \quad (77)$$

where the temporal weighting is flat, and $\{w_x(m)\}$ are real positive spatial error weights, which sum to 1. The error can be expressed as

$$e = \frac{1}{N} \sum_{n,m} w_x(m) \left| p(n, m) - \sum_k a_1(k) \exp(i\alpha_k n) b(k, m; u_1, u_2, G, \lambda) \right|^2, \quad (78)$$

where $b(k, m) = b(k, m; u_1, u_2, G, \lambda)$ is given by

$$b(k, m; u_1, u_2, G, \lambda) \equiv \exp[-i\alpha_k \beta(m) u_1] + G \exp[-i\alpha_k \lambda - i\alpha_k \beta(m) u_2]. \quad (79)$$

Defining difference

$$d(n, m) = p(n, m) - \sum_k a_1(k) \exp(i\alpha_k n) b(k, m) \quad (80)$$

then yields, from equations (78) and (51),

$$e = \sum_m w_x(m) \frac{1}{N} \sum_n |d(n, m)|^2 = \sum_m w_x(m) \frac{1}{N^2} \sum_l |D(l, m)|^2. \quad (81)$$

Now, from equations (80) and (50),

$$\begin{aligned} \frac{1}{N} D(l, m) &= \frac{1}{N} \sum_{n=0}^{N-1} \exp\left(-i \frac{2\pi n l}{N}\right) d(n, m) \\ &= \frac{1}{N} \sum_n \exp\left(-i \frac{2\pi n l}{N}\right) \left[p(n, m) - \sum_k a_1(k) \exp\left(i \frac{2\pi k n}{N}\right) b(k, m) \right] \\ &= q(l, m) - a_1(l) b(l, m), \end{aligned} \quad (82)$$

where the $\{q(l, m)\}$ are the temporal discrete Fourier transforms

$$q(l, m) = \frac{1}{N} \sum_{n=0}^{N-1} \exp(-i 2\pi n l / N) p(n, m), \quad \text{for } l = 0:N-1, \quad m = 0:M-1. \quad (83)$$

Therefore, equation (81) for the average error becomes

$$e = \sum_m w_x(m) \sum_l |q(l, m) - a_1(l) b(l, m)|^2. \quad (84)$$

To minimize e , consider the partial derivative

$$\frac{\partial e}{\partial a_1^*(k)} = - \sum_m w_x(m) [q(k, m) - a_1(k) b(k, m)] b^*(k, m) \quad (85)$$

for $k = k_a : k_b$. The conditionally optimal coefficients are explicitly

$$a_1(k) = \frac{\sum_m w_x(m) q(k, m) b^*(k, m)}{\sum_m w_x(m) |b(k, m)|^2} \quad \text{for } k = k_a : k_b. \quad (86)$$

These solutions are decoupled in k because of the flat temporal weighting and $1/T$ frequency separation. Substituting equation (86) into equation (84) yields the conditionally minimal error

$$\begin{aligned} e &= \sum_m w_x(m) \sum_k [q(k, m) - a_1(k) b(k, m)] q^*(k, m) \\ &= \sum_m w_x(m) \sum_k |q(k, m)|^2 - \sum_k a_1(k) \sum_m w_x(m) b(k, m) q^*(k, m) \\ &= \sum_m w_x(m) \sum_k |q(k, m)|^2 - \sum_k \frac{\left| \sum_m w_x(m) q(k, m) b^*(k, m) \right|^2}{\sum_m w_x(m) |b(k, m)|^2}. \end{aligned} \quad (87)$$

Recall (from equations (75) and (79)) that

$$\begin{aligned} b(k, m) &= b(k, m; u_1, u_2, G, \lambda) \\ &= \exp[-i\alpha_k \beta(m) u_1] + G \exp[-i\alpha_k \lambda - i\alpha_k \beta(m) u_2]. \end{aligned} \quad (88)$$

The leading term in equation (87) is independent of hypothesized values u_1 , u_2 , G , and λ . To further minimize \underline{e} , the quantity

$$r(u_1, u_2, G, \lambda) \equiv \sum_{k=k_a}^{k_b} \frac{\left| \sum_{m=0}^{M-1} w_x(m) q(k, m) b^*(k, m) \right|^2}{\sum_{m=0}^{M-1} w_x(m) |b(k, m)|^2} \quad (89)$$

must be maximized by choice of u_1 , u_2 , G , and λ . The sum over k (frequency bin number) reflects an incoherent addition, because no phase relationships are assumed between individual frequency components in the received data. The numerator sum over m (spatial element number) is a coherent addition when the latter four parameters of $b(k, m; u_1, u_2, G, \lambda)$ line up with the *actual* parameter values in FFT data $\{q(k, m)\}$. The denominator sum over m in equation (89) is a normalization factor, which depends on k , the frequency bin number, in addition to u_1 , u_2 , G , and λ .

Letting

$$F(k) \equiv \sum_m w_x(m) |q(k, m)|^2 \quad \text{for } k = k_a : k_b, \quad (90)$$

allows equation (87) to be written as

$$\underline{e} = \sum_k F(k) (1 - \rho_k), \quad (91)$$

where

$$\rho_k = \frac{\left| \sum_m w_x(m) b^*(k, m) q(k, m) \right|^2}{\sum_m w_x(m) |b(k, m)|^2 \sum_m w_x(m) |q(k, m)|^2}. \quad (92)$$

By Schwartz's inequality, $0 \leq \rho_k \leq 1$ for all k .

Form (92) is an interesting one, but equation (89) is the preferred form to maximize. The "probe" function $b(k, m; u_1, u_2, G, \lambda)$ in equation (88) is a function of the four real parameters u_1 , u_2 , G , and λ ; therefore, a four-dimensional search for the maximum of r in equation (89) is required. More generally, G could be complex, if desired; then a five-dimensional real search on r in equation (89) would be needed.

Once the optimal parameter values (\hat{u}_1 , \hat{u}_2 , \hat{G} , $\hat{\lambda}$) that maximize r in equation (89) have been determined, the optimum amplitudes follow from equations (85) and (78) as

$$\hat{a}_1(k) = \frac{\sum_m w_x(m) q(k, m) \hat{b}^*(k, m)}{\sum_m w_x(m) |\hat{b}(k, m)|^2} \quad \text{for } k = k_a : k_b, \quad (93)$$

where

$$\hat{b}(k, m) = \exp[-i\alpha_k \beta(m) \hat{u}_1] + \hat{G} \exp[-i\alpha_k \hat{\lambda} - i\alpha_k \beta(m) \hat{u}_2]. \quad (94)$$

The minimal residual in the frequency-space domain can be obtained from equation (84) in the form

$$\hat{q}(k, m) = q(k, m) - \hat{a}_1(k) \hat{b}(k, m). \quad (95)$$

5. BEAMFORMING FOR A SINGLE MOVING SOURCE NEAR AN ARBITRARY PLANAR ARRAY

5.1 THEORY

It is assumed that a source moves from (x_1, y_1) to (x_2, y_2) during an observation time T , with constant speed in a straight line (see figure 22). The range from the source to the receiving array is arbitrary; also,

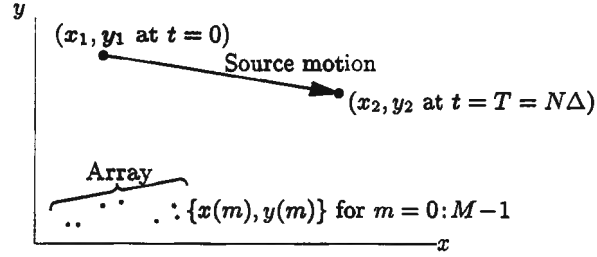


Figure 22. Sensor and Target Motion

the range and angle of the source can vary during the observation time T . Samples are taken at times $n\Delta$, where $n = 0:N-1$ and Δ is the time-sampling increment. The source location at time $t = n\Delta$ is

$$x_s(n) = x_1 + n \frac{x_2 - x_1}{N-1}, \quad (96)$$

$$y_s(n) = y_1 + n \frac{y_2 - y_1}{N-1}. \quad (97)$$

It is also assumed that there are M receivers placed at coordinates $\{x(m), y(m)\}$, with $m = 0:M-1$. The separation distance between the single source and the m -th receiving element at time $n\Delta$ is

$$s(n, m) = \left\{ [x_s(n) - x(m)]^2 + [y_s(n) - y(m)]^2 \right\}^{\frac{1}{2}}. \quad (98)$$

The separation distance $s(n, m)$ is a function of x_1, y_1, x_2 , and y_2 , as well as a function of n and m .

Modeling the source as transmitting a waveform composed of a sum of single frequencies yields the corresponding received waveform as:

$$\sum_{k=k_a}^{k_b} a(k) \exp(i 2\pi f_k t), \quad (99)$$

where the $\{a(k)\}$ are complex strength coefficients. The fitting frequencies selected will be

$$f_k = \frac{k}{T} = \frac{k}{N\Delta} \quad \text{for } k = k_a : k_b, \quad (100)$$

although no simplification results from this choice. Thus, the received waveform samples are modeled at time $n\Delta$ and element m as

$$\begin{aligned}\tilde{p}_1(n\Delta, x(m)) &= \sum_{k=k_a}^{k_b} a(k) \exp\left\{i 2\pi f_k \left[n\Delta - \frac{1}{c} s(n, m)\right]\right\} \\ &= \sum_{k=k_a}^{k_b} a(k) \exp\left\{i \alpha_k [n - h(n, m)]\right\}, \quad \alpha_k = \frac{2\pi k}{N},\end{aligned}\quad (101)$$

where the dimensionless quantity

$$h(n, m) = \frac{s(n, m)}{c\Delta}, \quad (102)$$

and c is the propagation speed.

The total weighted squared error between this model and the actual received data $\{p(n, m)\}$ is

$$e = \sum_{n=0}^{N-1} \sum_{m=0}^{M-1} w_t(n) w_x(m) \left| p(n, m) - \sum_{k=k_a}^{k_b} a(k) \exp\left\{i \alpha_k [n - h(n, m)]\right\} \right|^2, \quad (103)$$

where a set of (positive real) temporal weights $\{w_t(n)\}$ and (positive real) spatial weights $\{w_x(m)\}$ are allowed. For fixed hypothesized x_1, y_1, x_2 , and y_2 , the set of amplitude coefficients $\{a(k)\}$ that minimizes error e is to be found. Finding these coefficients requires differentiation of error e with respect to each of the amplitude strengths, indexed by \underline{k} :

$$\begin{aligned}\frac{\partial e}{\partial a^*(\underline{k})} &= - \sum_{n,m} w_t(n) w_x(m) \left[p(n, m) - \sum_k a(k) \exp\left\{i \alpha_k [n - h(n, m)]\right\} \right] \\ &\quad \times \exp\left\{-i \alpha_{\underline{k}} [n - h(n, m)]\right\} \\ &= - \sum_{n,m} w_t(n) w_x(m) p(n, m) \exp\left\{-i \frac{2\pi \underline{k}}{N} [n - h(n, m)]\right\} \\ &\quad + \sum_k a(k) \sum_{n,m} w_t(n) w_x(m) \exp\left\{-i \frac{2\pi}{N} (\underline{k} - k) [n - h(n, m)]\right\} \\ &= -P(\underline{k}) + \sum_{k=k_a}^{k_b} a(k) W(\underline{k} - k) \quad \text{for } \underline{k} = k_a : k_b,\end{aligned}\quad (104)$$

where

$$P(k) = \sum_{n,m} w_t(n) w_x(m) p(n, m) \exp\left\{-i \frac{2\pi k}{N} [n - h(n, m)]\right\}, \quad (105)$$

$$W(k) = \sum_{n,m} w_t(n) w_x(m) \exp\left\{-i \frac{2\pi k}{N} [n - h(n, m)]\right\}. \quad (106)$$

The last quantity is defined only for $|k| \leq k_b - k_a$. $W(k)$ possesses no δ -function properties, regardless of the choices of weights $\{w_t(n)\}$ and $\{w_x(m)\}$, due to the nonlinear function $h(n, m)$.

The conditionally optimal coefficients $\{\underline{a}(k)\}$ are found by setting all the derivatives in equation (104) equal to zero:

$$\sum_{k=k_a}^{k_b} W(\underline{k}-k) \underline{a}(k) = P(\underline{k}) \quad \text{for } \underline{k} = k_a : k_b. \quad (107)$$

Equation (107) comprises K simultaneous linear equations, where $K = k_b - k_a + 1$. The matrix $[W(\underline{k}-k)]$ is Hermitian Toeplitz and is of size $K \times K$. The corresponding conditionally minimal error \underline{e} is calculated from equations (103) and (105):

$$\begin{aligned} \underline{e} &= \sum_{n,m} w_t(n) w_x(m) \left[p(n,m) - \sum_k \underline{a}(k) \exp\{i \alpha_k [n - h(n,m)]\} \right] p^*(n,m) \\ &= \sum_{n,m} w_t(n) w_x(m) |p(n,m)|^2 - \sum_k \underline{a}(k) P^*(k). \end{aligned} \quad (108)$$

To further minimize \underline{e} requires maximization of

$$r(x_1, y_1, x_2, y_2) \equiv \sum_{k=k_a}^{k_b} \underline{a}(k) P^*(k). \quad (109)$$

Letting

$$\mathbf{W}_{K \times K} = [W(\underline{k}-k)], \quad \mathbf{a}_{K \times 1} = [\underline{a}(k_a) \cdots \underline{a}(k_b)]^T, \quad \mathbf{P}_{K \times 1} = [P(k_a) \cdots P(k_b)]^T, \quad (110)$$

results in equations (107) and (109) yielding

$$\mathbf{W} \mathbf{a} = \mathbf{P}, \quad \mathbf{a} = \mathbf{W}^{-1} \mathbf{P}, \quad r = \mathbf{P}' \mathbf{a} = \mathbf{P}' \mathbf{W}^{-1} \mathbf{P}, \quad (111)$$

where the prime denotes conjugate transpose. Vector \mathbf{P} and square matrix \mathbf{W} are functions of x_1, y_1, x_2 , and y_2 . The required procedure is now to search for a maximum of equations (109) or (111) in x_1, y_1, x_2 , and y_2 space, where $\{\underline{a}(k)\}$ are the solutions to equation (107). The Hermitian Toeplitz character of \mathbf{W} can be used to facilitate solving equation (107), rather than explicitly calculating its inverse.

Explicitly, for $n = 0:N-1$ and $m = 0:M-1$,

$$h(n, m) = \frac{1}{c\Delta} \left\{ \left[x_1 + n \frac{x_2 - x_1}{N-1} - x(m) \right]^2 + \left[y_1 + n \frac{y_2 - y_1}{N-1} - y(m) \right]^2 \right\}^{\frac{1}{2}}. \quad (112)$$

For *each* hypothesized x_1, y_1, x_2 , and y_2 , calculation of equation (112) requires evaluation of NM terms. Next, equations (105) and (106) each require K summations of size NM . Then, equation (107) requires the solution of K simultaneous linear equations with a Hermitian Toeplitz kernel. Finally, equation (109) is a sum of K complex terms, resulting in a real quantity.

The quantity $r(x_1, y_1, x_2, y_2)$ in equation (109) is maximized at position estimates $\hat{x}_1, \hat{y}_1, \hat{x}_2$, and \hat{y}_2 . First, these best position estimates are substituted into equation (110), and matrix $\hat{\mathbf{W}}$ and vector $\hat{\mathbf{P}}$ are evaluated. Then, $\hat{\mathbf{W}} \hat{\mathbf{a}} = \hat{\mathbf{P}}$ is solved for optimum amplitudes $\{\hat{a}(k)\}$. Finally, the minimal time-space residual can be deduced from equation (108) in the form

$$\hat{p}(n, m) = p(n, m) - \sum_k \hat{a}(k) \exp\{i \alpha_k [n - \hat{h}(n, m)]\}, \quad (113)$$

where $\hat{h}(n, m)$ follows obviously from equation (112). There is no simple relation for the minimal frequency-space residual $\hat{q}(k, m)$ because of the nonlinear dependence of $\hat{h}(n, m)$ on n .

5.2 IMPLEMENTATION

The theory outlined in the last section was implemented in a MATLAB program and tested on simulated data for a variety of scenarios.

5.2.1 Data Simulation

The first step was to generate the data that an array of sensors would produce in the presence of a moving source. The starting positions and ending positions were defined as x_1 , y_1 , x_2 , and y_2 .

```
%starting position:
x1 = 110;
y1 = 110;
%ending position:
x2 = 100;
y2 = 120;
```

The basic parameters were set as follows:

```
c = 1500;      % wavespeed (m/s)
T = 20;        % total duration of data (s)
speed = 5;     % speed of source (m/s)
dt = .1;       % sampling increment (s)
ka = 100;      % starting frequency index
kb = 110;      % ending frequency index
M = 8;         % total number of sensors
dx = 3.75;     % spacing of hydrophones (m)
xarray = dx*(0:M-1);
yarray = zeros(size(xarray));
N = T/dt;      % total number of time samples
a = ones(size(ka:kb)); % Frequency components:
d = speed*T;   % distance traveled by source (m)
```

Some variation in the y positions of the receiving array elements was added to break the linearity of the array and the resulting left-right ambiguity. The array elements were shifted in a random way. The random number generator was reset to its initial value so that the same array would be used each time the program was run.

```
randn('state',0)
sigmay = 1 % (m)
yarray = yarray + sigmay*randn(size(yarray));
```

Various matrices are now set up in which the columns correspond to the different elements of the receiving array, and the rows correspond to the different time samples. First, "matrix" versions of the element locations are set up, as follows:

```

xm = ones(N,1)*xarray;
ym = ones(N,1)*yarray;

```

Then, matrices of indices, which will be used later, are set up. These matrices, m and n , are arranged such that the elements of m vary only across its columns and the elements of n vary only down its rows:

```

[m,n] = meshgrid(0:(M - 1),0:(N - 1));

```

For example, the first few elements of m and n are

```

>> m(1:3,1:3)
ans =
     0     1     2
     0     1     2
     0     1     2
>> n(1:3,1:3)
ans =
     0     0     0
     1     1     1
     2     2     2

```

These matrices can then be used in a “vectorized” sense to calculate quantities such as the source location at each timestep:

```

xsn = x1 + n*(x2 - x1)/(N - 1);
ysn = y1 + n*(y2 - y1)/(N - 1);

```

The dimensionless separation distance between the source and the m -th receiving element at timestep n can be calculated according to:

```

hnm = sqrt((xsn - xm).^2 + (ysn - ym).^2)/(c*dt);

```

This calculation corresponds to equation (112). A for-loop is used to add the frequency components to obtain the signal received by each element at each time step:

```

pnm = 0;
k = ka:kb;
i = sqrt(-1);
twopioverN = 2*pi/N;
for this_k = 1:length(k)
    alphak = twopioverN*k(this_k);
    pnm = pnm + a(this_k)*exp(alphak*(n - hnm)*i);
end

```

The matrix `pnm` is the data matrix, in which time runs down the rows and the hydrophone number runs across the columns.

Next, the option of adding some complex normally-distributed random noise using the `randn` function is available:

```
snr = 0; % dB
Noise = randn(size(pnm)) + i*randn(size(pnm));
As = mean(std(pnm));
An = mean(std(Noise));
NoiseScaleFactor = As / (An*10^(snr/20));
pnm = pnm + Noise * NoiseScaleFactor;
```

5.2.2 Example

An example of the output produced by the simulation coding is shown in figure 23, where a linear receiving array of $M = 10$ sensors is seen in the top plot. The source emitted a single frequency tone, and moved from the beginning of the arrow to the end of the arrow during the acquisition time. The lower two plots show the signal received at each of the elements during a short period at the beginning of the acquisition time (left) and at the end (right). The light and dark strips represent the peaks and troughs of the received waveform. At the beginning of the acquisition time, the curved wavefronts arrive at the elements near the middle of the array first. The wavefronts can be imagined as a series of concentric circles emanating from the tail of the arrow. At the end of the acquisition time, the curved wavefronts arrive at element 10 first and then propagate down the array towards element 1. In this case, the wavefronts can be imagined as a series of concentric circles emanating from the head of the arrow. An animation of the strip display would show, at the start of the acquisition, the wavefronts meeting the array first at the middle of the array (plot at left). Then, as time elapsed, the wavefronts would meet the array at

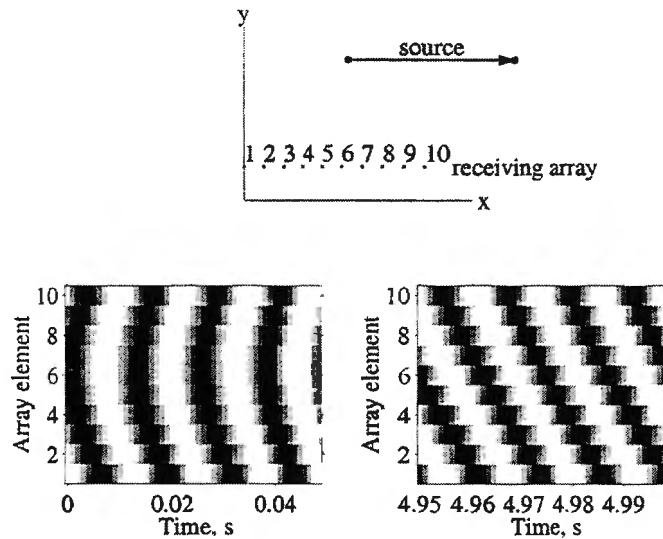


Figure 23. Simulated Data

points progressively closer to element 10 (plot at right). The optimization algorithm amounts to fitting a modeled sum of frequencies to these data by choosing the best start and end points for the arrow (x_1 , y_1 , x_2 , and y_2).

5.3 OPTIMIZATION ALGORITHM

The driver code for the optimization used the MATLAB function `fminsearch` to do the minimization. This function employed the Nelder-Mead simplex (direct search) method for multidimensional, unconstrained nonlinear minimization.⁷ The algorithm returns a vector that is a local minimizer of the function `movingsourceerror` near the starting vector `guess`:

```
guess = [xguess1 yguess1 xguess2 yguess2];
opts = optimset('MaxIter',2000,'MaxFunEvals',2000);
x = fminsearch('movingsourceerror',guess,opts);
```

The variable `opts` controls the maximum allowable number of iterations and function evaluations.

The function `movingsourceerror` contains the code that first finds the optimal coefficients \underline{a}_k by solving the simultaneous equation (107), and then uses these coefficients to calculate the quantity $r(x_1, y_1, x_2, y_2)$ given by equation (109). The code begins by defining the time and space weighting functions as:

```
wt = ones(1,N)/N;
wx = ones(1,M)/M;
```

It then computes the quantity $h(n, m)$ based on the parameters x_1 , y_1 , x_2 , and y_2 , which are given as input arguments to the function:

```
hnm = sqrt((x1 + n*(x2 - x1)/(N - 1) - xm).^2 + ...
           (y1 + n*(y2 - y1)/(N - 1) - ym).^2)/(c*dt);
```

The matrix W is a function of $(\underline{k} - k)$, with a sum over m and n required to calculate each element. Because all the dimensions for standard MATLAB two-dimensional matrices have been used, one must index over n and m and use a matrix to represent $(\underline{k} - k)$. Two `for`-loops can then be used to perform the summation over n and m :

```
kbar = k;
[K,Kbar] = meshgrid(k,kbar);
W = 0;
P = 0;
KbarminusK = Kbar - K;
```

Since there is no zero index in MATLAB, loops going from `nn = 1:N`, etc., are used as matrix indices, whereas `nn-1` etc., are used in the calculations:

```

for mm = 1:M
  for nn = 1:N
    fact = -2*pi*((nn - 1) - hnm(nn,mm))/N;
    weight = wt(nn)*wx(mm);
    W = W + weight*exp(fact*KbarminusK*i);
    P = P + weight*exp(fact*k*i)*pnm(nn,mm);
  end
end
end

```

The theory above has P as a column vector; therefore, the transpose

```
P = P.';
```

is chosen. Now the equation $WA = P$ is solved to obtain the least-squares coefficients, $\{\underline{a}(k)\}$, which will be returned in the vector A :

```
A = W\P;
```

Having found the conditionally optimal $\{\underline{a}(k)\}$, r must be maximized to minimize the error \underline{e} . However, because a minimizer is being used, the sign must be changed:

```
r = -real(P'*A);
```

(The imaginary part of r in equation (109) should be zero; therefore, the smallness of the magnitude of the imaginary part of r forms a partial check on the accuracy of the final solution.)

5.4 RESULTS

5.4.1 Examination of the Error Function

The minimal error \underline{e} given in equation (108) can be considered as a scalar function of (x_1, y_1, x_2, y_2) . To understand the behavior of this (four-dimensional) function, \underline{e} is calculated as a function of either the start-point coordinates with the end point fixed, or as a function of the end-point coordinates with the start point fixed, both of which are two-dimensional "slices" through the four-dimensional function. Two cases are considered: in one, the source moves in the nearfield of the array, and in the other, the source moves in the farfield of the array.

5.4.1.1 Nearfield Scenario. Figure 24 shows the variation in the conditionally minimal error \underline{e} with changes in the modeled start and end points of the trajectory. The upper plots show contours of the error quantity \underline{e} . The lower plots show the same quantity plotted as surfaces. Two scenarios are illustrated. The plots on the left (top and bottom) show \underline{e} as a function of (x_1, y_1) with x_2 and y_2 held fixed at their true values, and the plots on the right (top and bottom) show \underline{e} as a function of (x_2, y_2) with x_1 and y_1 held fixed at their true values. Contours are drawn at the same levels in both contour plots. The dots show the positions of the sensor array, and the arrow shows the true trajectory of the source during the observation period. In both scenarios, there is a deep minimum in the region within roughly a wavelength of the true value. (These runs simulated a noise-free, single planewave, with $k = 400$, and $T = 5$ s, yielding a wavelength of 18.75 m.) Although a line array receiver was used, the resulting \underline{e} is not expected to be left-right symmetric because the other end of the trajectory was held fixed; therefore, the left-right symmetric point would represent a completely different source trajectory that is easily ‘rejected’ by the fitting process. The error function *would* be left-right symmetric if either end of the trajectory lay along the axis of the array. Outside the region within a wavelength of the true solution, the error function is relatively flat and appears to contain many shallow local minima. This kind of function may present a challenge to the minimization algorithm chosen, especially in the presence of noise.

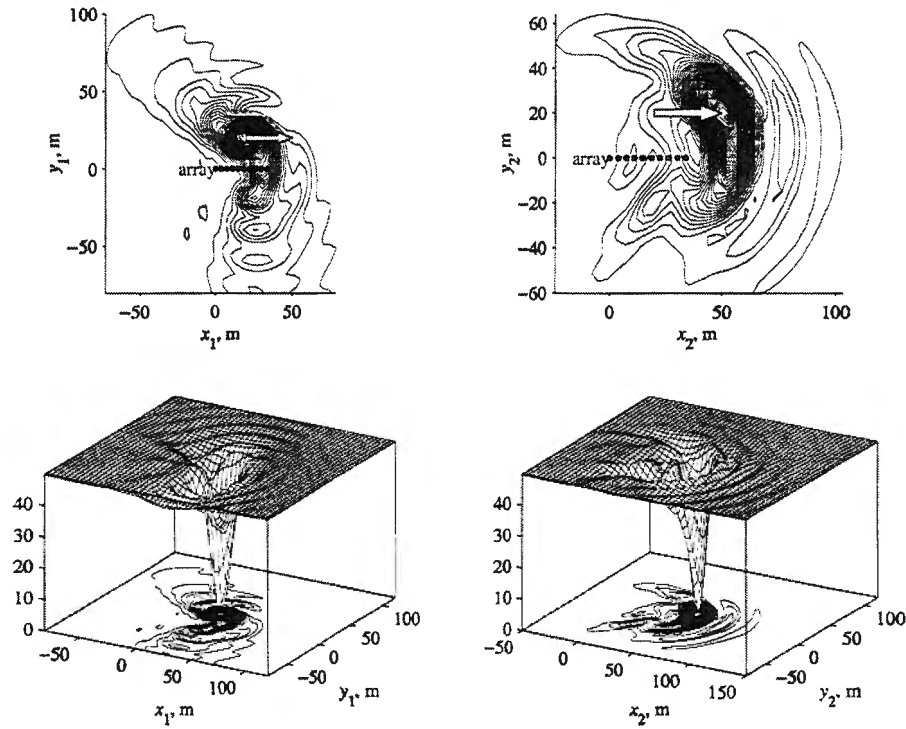


Figure 24. Error for Nearfield Scenario

5.4.1.2 Farfield Scenario. Figure 25 shows the same type of results as figure 24, except this time the source is at a greater distance from the array. The error function has a narrow valley that follows an arc centered near the location of the array. Again, this kind of function may present a challenge to the minimization algorithm chosen, especially in the presence of noise.

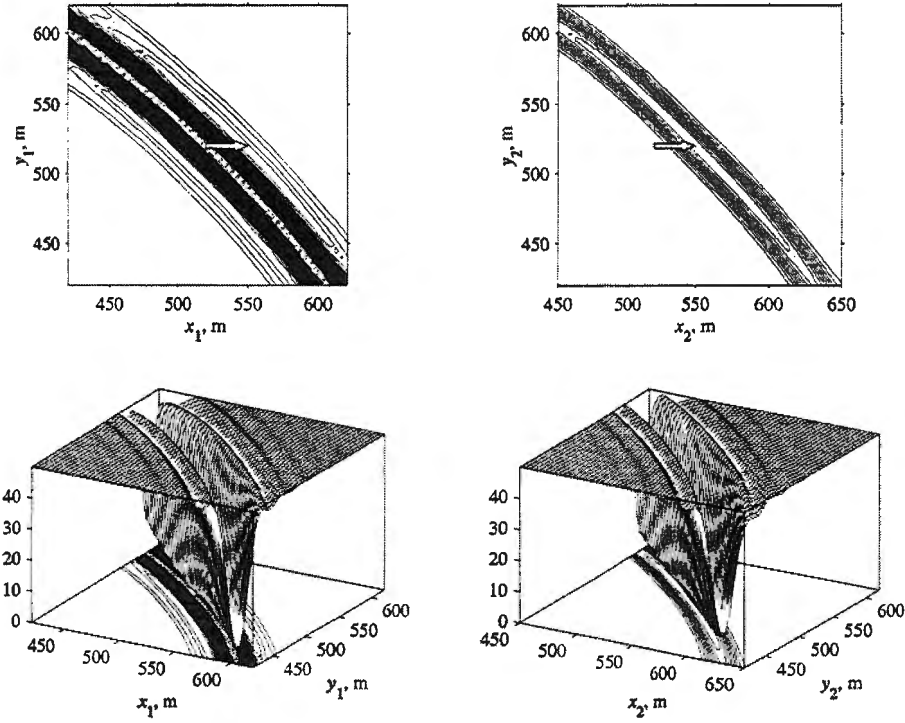


Figure 25. Error for Farfield Scenario

5.4.2 Fitted Trajectories with Noisy Data

Simulations in this section were carried out using the scenario shown in figure 26. An array of eight elements was located along the x -axis, with each element equally spaced at a separation distance of 3.75 m. The first element of the array was located at the origin. A source moving in the nearfield of the array (as shown by the thick arrow indicated on the plot) emitted frequencies $f_k = k/T$, where $k = k_a:k_b$, $k_a = 100$, $k_b = 110$, and $T = 20$ s. The speed of the source was such that it moved from $(x_1, y_1) = (60, 60)$ to $(x_2, y_2) = (50, 70)$ during the time interval $T = 20$ s. The propagation speed was taken to be 1500 m/s. The time between samples was $\Delta = 0.1$ s, resulting in $N = 200$ samples per element. Noise was added to the pressure data at various SNRs; the SNR is defined in the same way as on page 42. A search was carried out for the values of x_1 , y_1 , x_2 , and y_2 that minimized \underline{g} , as described above. Five realizations of the random noise field were used at each SNR. The values used to initialize the search, which remained constant throughout these runs, consisted of motion beginning at a range of 500 m at a bearing equal to $\tan^{-1} \{ [(y_1 + y_2)/2] / [(x_1 + x_2)/2] \}$ and finishing at the position reached after traveling for time T at 10 knots towards the origin. The numerical values were $x_1 = 323.0$, $y_1 = 382.0$, $x_2 = 257.0$, and $y_2 = 303.0$. The results of the minimizations are shown by the thin arrows, with the size of the arrowheads being inversely proportional to the SNR, as indicated on the legend.

The data of figure 26 are presented as individual coordinate errors and as functions of SNR in figure 27. The four plots show the magnitude of the difference, in meters, between the coordinates obtained from the search and the true coordinates, as a function of SNR. The results show that, even for this close-range case (85 m), an error on the order of 10 m remains for SNRs less than about 40 dB.

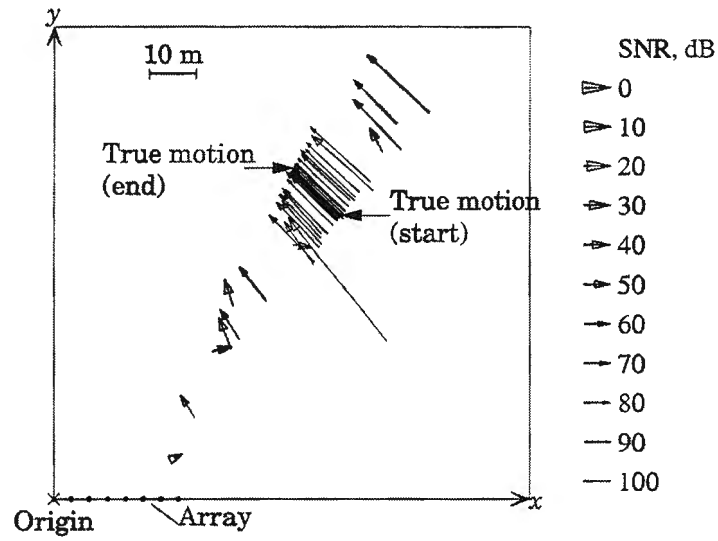


Figure 26. True Trajectory and Fitted Trajectories for Scenarios with Various SNRs

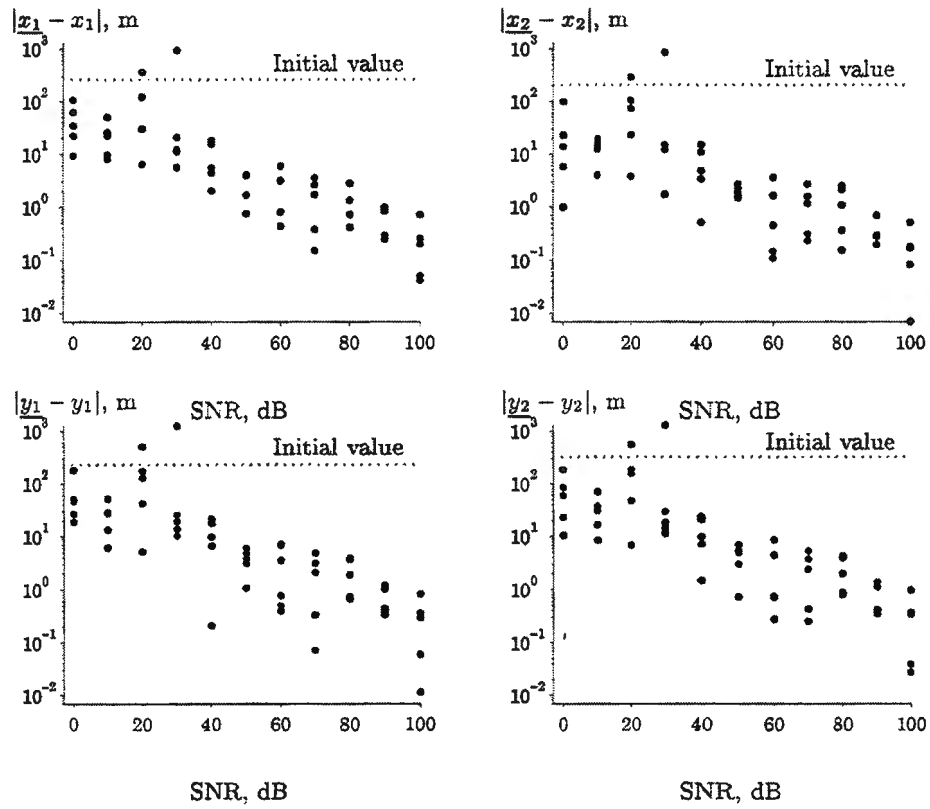


Figure 27. Fitted Coordinate Errors Plotted Against SNR

5.4.3 Comparison with Conventional Beamformer

The new algorithm has the potential to outperform beamformers because it yields tracking information directly; in conventional sonar systems, tracking is performed only after a set of peaks in the beamformed data has been obtained. But, for a moving source, such peaks may never be detected because the beamformer "peak" will be smeared out over the range of angles swept out by the moving source during the integration time of the beamformer. An example of this can be seen in figure 28. The plots at the top are for a stationary source, and the plots at the bottom are for a moving source. The beamformed output for the stationary source shows a single peak at the correct bearing, but the beamformed output for the moving source shows energy spread out over the angles swept out by the source as it moves during the time over which the data were acquired (depicted by the gray areas). The output in this case could be mistaken for a pair of stationary sources. It is also possible that an automatic detector would not yield a detection for the moving case because of its high sidelobe level.

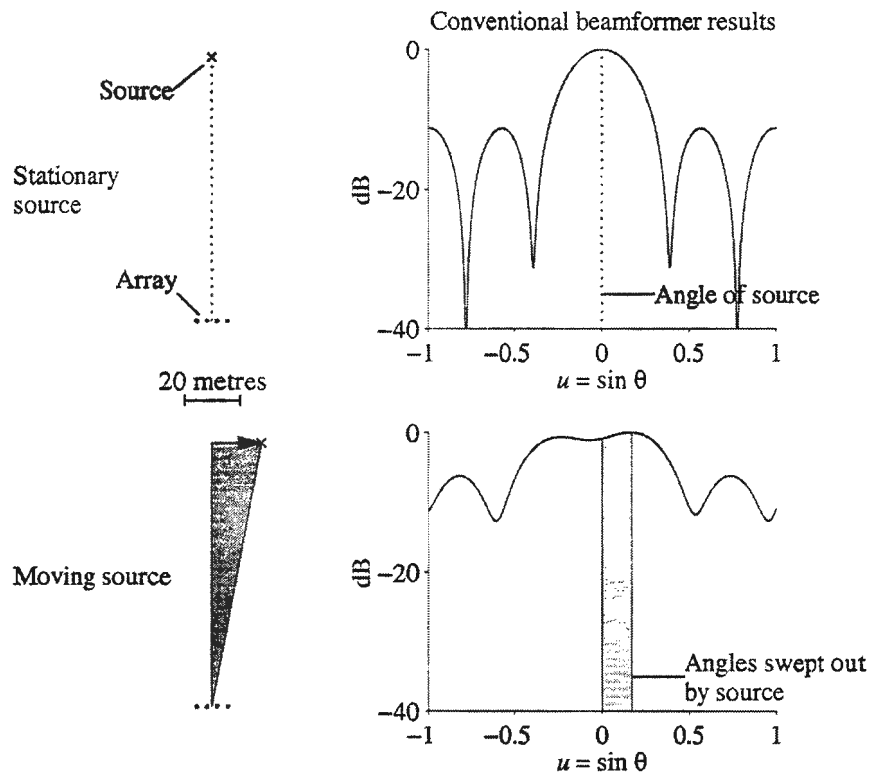


Figure 28. Conventionally Beamformed Results for a Stationary Source (Top) and a Moving Source (Bottom)

6. CONCLUSIONS

A new array processing technique has been presented that allows optimal source amplitudes and arrival angles to be determined from data produced by arbitrary arrays. Used to fit either one or two planewaves to arbitrarily spaced linear array data, the technique has shown superior performance to conventional beamforming when more than one source is within the beamwidth of an array. With such situations becoming more likely as operating frequencies are driven to lower values, in an effort to increase detection ranges, the approach can be used to coherently subtract strong arrivals from received data, allowing the detection of additional weak arrivals in close angular proximity.

When a planewave arrives at an arbitrary two-dimensional array from a moving source, a similar technique yields optimal values of the source amplitudes of the planewave, as well as the starting and ending positions of the moving source. The new processing thus performs the functions of a combined beamformer and tracker in such a way that the total error over the array and the observation interval is minimized.

The results presented here are for simulated data. Future work will involve the application of these methods to measured at-sea data. A further issue to be addressed is the adequacy of the four-dimensional iterative minimization procedures.

APPENDIX

ALTERNATIVE FORMULATION OF TWO-PLANEWAVE FIT

There is an alternative formulation to the two-planewave fitting waveform in equation (46) that is exact for all u_1, u_2 and does not develop any singularities as $u_1 \rightarrow u_2$. Letting central angle u_c and difference angle ϵ be defined as

$$u_c = (u_1 + u_2)/2, \quad \epsilon = u_1 - u_2, \quad (\text{A-1})$$

in terms of the original arrival angles u_1 and u_2 (difference angle ϵ need not be small), then, by using $u_1 = u_c + \epsilon/2$, $u_2 = u_c - \epsilon/2$, the k -th frequency component of the original model (equation (46)) can be expressed as

$$t_k = \left[b_1(k) B_1(k, m) + b_2(k) B_2(k, m) \right] \exp(i \alpha_k n) \quad \text{for } k = k_a : k_b, \quad (\text{A-2})$$

where

$$\left. \begin{aligned} \alpha_k &= \frac{2\pi k}{N}, \quad \beta_m = \frac{x(m)}{c\Delta}, \quad \text{sinx}(x) = \frac{\sin(x)}{x}, \\ B_1(k, m) &= \cos(\alpha_k \beta_m \epsilon/2) \exp(-i \alpha_k \beta_m u_c), \\ B_2(k, m) &= \beta_m \text{sinx}(\alpha_k \beta_m \epsilon/2) \exp(-i \alpha_k \beta_m u_c), \\ b_1(k) &= a_1(k) + a_2(k), \\ b_2(k) &= -i[a_1(k) - a_2(k)] \alpha_k \epsilon/2. \end{aligned} \right\} \quad (\text{A-3})$$

For the best fit of sum waveform $\sum_k t_k$ to a given data set $\{p(n, m)\}$, the optimal coefficients $\{b_1(k)\}$ and $\{b_2(k)\}$ in equation (A-2) will all be *finite*, regardless of the size of ϵ , including $\epsilon = 0$. However, because

$$a_1(k) = \frac{1}{2} b_1(k) + \frac{i b_2(k)}{\alpha_k \epsilon}, \quad a_2(k) = \frac{1}{2} b_1(k) - \frac{i b_2(k)}{\alpha_k \epsilon}, \quad (\text{A-4})$$

then $a_1(k) \rightarrow \infty$ and $a_2(k) \rightarrow \infty$ as $\epsilon \rightarrow 0$ in the original model (equation (46)). (This effect has been observed before and has been explained by Nuttall.⁸) On the other hand, the model formulation of equation (A-2) does not undergo this singular behavior for any ϵ .

As $\epsilon \rightarrow 0$, the model waveform $\sum_k t_k$ becomes

$$\sum_k [b_1(k) + b_2(k) \beta_m] \exp[i \alpha_k (n - \beta_m u_c)], \quad (\text{A-5})$$

upon use of equations (A-2) and (A-3). This dependence of the fit on m is different from the original model (equation (46)); such modified behavior has been described in eq. 28 *et seq.* and eq. 51 *et seq.* in Nuttall.⁸

When component form (A-2) is used to approximate the available data, the error to be minimized becomes, for flat temporal weighting,

$$e = \frac{1}{N} \sum_{n, m} \left| p(n, m) - \sum_{k=k_a}^{k_b} t_k \right|^2. \quad (\text{A-6})$$

Holding angles u_c and ϵ fixed for now, the partial derivatives of e with respect to $\{b_1(k)\}$ and $\{b_2(k)\}$ yield decoupled pairs of simultaneous linear equations for the conditionally best coefficients $\{b_1(k)\}$ and $\{b_2(k)\}$ as

$$\left. \begin{aligned} W_{11}(k) \underline{b}_1(k) + W_{12}(k) \underline{b}_2(k) &= Q_1(k) \\ W_{21}(k) \underline{b}_1(k) + W_{22}(k) \underline{b}_2(k) &= Q_2(k) \end{aligned} \right\} \text{ for } k = k_a : k_b, \quad (\text{A-7})$$

where

$$\left. \begin{aligned} W_{11}(k) &= \sum_m w_x(m) |B_1(k, m)|^2 = \sum_m w_x(m) \cos^2(\alpha_k \beta_m \epsilon / 2), \\ W_{22}(k) &= \sum_m w_x(m) |B_2(k, m)|^2 = \sum_m w_x(m) \beta_m^2 \sin^2(\alpha_k \beta_m \epsilon / 2), \\ W_{12}(k) &= W_{21}^*(k) = \sum_m w_x(m) B_1^*(k, m) B_2(k, m) \\ &= \sum_m w_x(m) \beta_m \sin(\alpha_k \beta_m \epsilon / 2) \cos(\alpha_k \beta_m \epsilon / 2), \\ Q_j(k) &= \sum_m w_x(m) q(k, m) B_j^*(k, m), \quad j = 1, 2. \end{aligned} \right\} \quad (\text{A-8})$$

It should be observed that all the $\{W_{ij}(k)\}$ are real functions of ϵ , but are independent of u_c and the data $\{p(n, m)\}$ or $\{q(k, m)\}$. The quantities $\{B_j(k, m)\}$ are complex functions of ϵ and u_c , but are independent of the data. The quantities $\{Q_j(k)\}$ are complex functions of ϵ and u_c as well as complex functions of the data.

The solutions to equation (A-7) are explicitly

$$\left. \begin{aligned} \underline{b}_1(k) &= \frac{W_{22}(k) Q_1(k) - W_{12}(k) Q_2(k)}{W_{11}(k) W_{22}(k) - W_{12}^2(k)} \\ \underline{b}_2(k) &= \frac{W_{11}(k) Q_2(k) - W_{12}(k) Q_1(k)}{W_{11}(k) W_{22}(k) - W_{12}^2(k)} \end{aligned} \right\} \text{ for } k = k_a : k_b. \quad (\text{A-9})$$

In the limit as $\epsilon \rightarrow 0$, it follows from equation (A-8) that the denominator of equation (A-9) tends to

$$\left(\sum_m w_x(m) \right) \left(\sum_m w_x(m) \beta_m^2 \right) - \left(\sum_m w_x(m) \beta_m \right)^2, \quad (\text{A-10})$$

which is *always* positive by Schwartz's inequality. Thus, equation (A-9) never develops any singularities for any value of ϵ ; that is, the denominator of equation (A-9) is never zero for any ϵ .

When the conditionally optimal coefficients in equation (A-9) are substituted in error expression (A-6), and equations (A-2) and (A-8) are employed, the conditionally optimal error becomes

$$\underline{e} = \frac{1}{N} \sum_{n, m} w_x(m) \left[p(n, m) - \sum_k \left\{ \underline{b}_1(k) B_1(k, m) + \underline{b}_2(k) B_2(k, m) \right\} \right] p^*(n, m) \quad (\text{A-11})$$

$$= \frac{1}{N} \sum_{n, m} w_x(m) |p(n, m)|^2 - \sum_k \left\{ \underline{b}_1(k) Q_1^*(k) + \underline{b}_2(k) Q_2^*(k) \right\} \quad (\text{A-12})$$

$$= \frac{1}{N} \sum_{n, m} w_x(m) |p(n, m)|^2 - r_2(u_c, \epsilon), \quad (\text{A-13})$$

where function

$$r_2(u_c, \epsilon) = \sum_{k=k_a}^{k_b} \frac{W_{22}(k)|Q_1(k)|^2 + W_{11}(k)|Q_2(k)|^2 - 2W_{12}(k)\Re\{Q_1^*(k)Q_2(k)\}}{W_{11}(k)W_{22}(k) - W_{12}^2(k)}, \quad (\text{A-14})$$

and \Re denotes the real part. To further minimize conditional error \underline{e} , the quantity $r_2(u_c, \epsilon)$ must now be maximized by choice of central angle u_c and difference angle ϵ ; see equation (A-1). No singularities develop in $r_2(u_c, \epsilon)$ for any value of ϵ , including $\epsilon = 0$.

Consideration of equation (A-8) reveals that $\{W_{ij}(k)\}$ are real functions of ϵ and k ; therefore, their values could be precalculated and stored, at least for a preliminary coarse search where difference angle ϵ could be fixed. Similarly, the quantities $\{B_j(k, m)\}$ in equation (A-3) are complex functions of ϵ and u_c , but are independent of the data $\{p(n, m)\}$ or $\{q(k, m)\}$. For a fixed ϵ , $\{B_j(k, m)\}$ could also be stored; the size of the storage would be KMM_c , where K is the number of frequency components in the original model (equation (46)), M is the number of array elements, and M_c is the number of central angles u_c of interest. On the other hand, the quantities $\{Q_j(k)\}$ in equation (A-8) are complex functions of ϵ and u_c , as well as complex functions of the data $\{q(k, m)\}$, and cannot be precalculated.

Once the unconditionally optimal angles \hat{u}_c and $\hat{\epsilon}$ are found from the maximization of $r_2(u_c, \epsilon)$ in equation (A-14), these angles must be substituted into equation (A-3) to obtain $\{\hat{B}_j(k, m)\}$, and then into equation (A-8) to obtain $\{\hat{W}_{ij}(k)\}$ and $\{\hat{Q}_j(k)\}$. Finally, equation (A-9) yields the best coefficient values $\{\hat{b}_j(k)\}$, where all the quantities must have their optimal (*) values.

The minimal residual in the time-space domain follows from equations (46) and (A-2) as

$$\hat{p}(n, m) = p(n, m) - \tilde{p}_2(n\Delta, x(m)) \quad (\text{A-15})$$

$$= p(n, m) - \sum_k \left[\hat{b}_1(k)\hat{B}_1(k, m, \hat{\epsilon}, \hat{u}_c) + \hat{b}_2(k)\hat{B}_2(k, m, \hat{\epsilon}, \hat{u}_c) \right] \exp(i\alpha_k n) \quad (\text{A-16})$$

for $n = 0:N-1$, $m = 0:M-1$. The corresponding minimal residual in the frequency-space domain is simply

$$\hat{q}(k, m) = q(k, m) - \hat{b}_1(k)\hat{B}_1(k, m, \hat{\epsilon}, \hat{u}_c) - \hat{b}_2(k)\hat{B}_2(k, m, \hat{\epsilon}, \hat{u}_c) \quad (\text{A-17})$$

for $k = k_a:k_b$, $m = 0:M-1$. These two forms of coherent subtraction should be employed using coefficients $\{\hat{b}_j(k)\}$ rather than resorting to the original model (equation (46)) and coefficients $\{a_j(k)\}$ from equation (A-4). The latter coefficients will be extremely large for very small ϵ and will cause loss of significance in residuals $\{\hat{p}(n, m)\}$ and $\{\hat{q}(k, m)\}$.

If $\hat{\epsilon}$ is not very small, the optimal amplitudes in the original model (equation (46)) can be found from equation (A-4) as

$$\hat{a}_1(k) = \frac{1}{2}\hat{b}_1(k) + \frac{i\hat{b}_2(k)}{\alpha_k\hat{\epsilon}}, \quad \hat{a}_2(k) = \frac{1}{2}\hat{b}_1(k) - \frac{i\hat{b}_2(k)}{\alpha_k\hat{\epsilon}}. \quad (\text{A-18})$$

This relation is exact and applies for all $\hat{\epsilon} \neq 0$.

This appendix has presented an alternative approach and solution to the two-planewave fitting procedure; all quantities are finite for all ϵ , except possibly for equation (A-18), which attempts a return to the amplitudes in the original model (equation (46)).

REFERENCES

1. S. M. Kay, *Fundamentals of Statistical Signal Processing: Estimation Theory*, Prentice Hall Inc., NJ, 1993.
2. A. H. Nuttall and J. H. Wilson, "Estimation of the Acoustic Field Directionality by Use of Planar and Volumetric Arrays Via the Fourier Series Method and the Fourier Integral Method," *Journal of the Acoustical Society of America*, vol. 90, no. 4, part 1, October 1991, pp. 2004–2019.
3. J. H. Wilson, "Applications of Inverse Beamforming Theory," *Journal of the Acoustical Society of America*, vol. 98, no. 6, December 1995, pp. 3250–3261.
4. I. S. D. Solomon, A. J. Knight, and M. V. Greening, "Sonar Array Signal Processing for Sparse Linear Arrays," *Fifth International Symposium on Signal Processing and Its Applications (ISSPA 99)*, vol. 2, August 1999, Brisbane, Australia, pp. 527–530.
5. I. S. D. Solomon, A. J. Knight, D. F. Liebing, and S. B. Faulkner, "Sonar Beamforming Using Fourier Integral Method," *Underwater Defence Technology (UDT) Conference (Pacific 2000)*, Sydney, Australia, February 2000, pp. 182–186.
6. I. S. D. Solomon and A. J. Knight, "Array Processing of Underwater Acoustic Sensors Using Weighted Fourier Integral Method," *10th IEEE Workshop on Statistical Signal and Array Processing*, Pocono Manor, Pennsylvania, 2000, pp. 707–711.
7. J. C. Lagarias, J. A. Reeds, M. H. Wright, and P. E. Wright, "Convergence Properties of the Nelder-Mead Simplex Algorithm in Low Dimensions," *Society for Industrial and Applied Mathematics Journal on Optimization*, vol. 9, no. 1, 1998, pp. 112–147.
8. A. H. Nuttall, "Weighted Least Squares Fit of a Real Tone to Discrete Data by Means of an Efficient Fast Fourier Transform Search," NUSC Technical Report 7785, Naval Underwater Systems Center, New London, CT, 27 August 1986, pp. 8–15.